



UNIVERSITY OF LEEDS

This is a repository copy of *MHD natural convection of Cu–Al₂O₃ water hybrid nanofluids in a cavity equally divided into two parts by a vertical flexible partition membrane*.

White Rose Research Online URL for this paper:
<http://eprints.whiterose.ac.uk/155110/>

Version: Accepted Version

Article:

Ghalambaz, M, Mehryan, SAM, Izadpanahi, E et al. (2 more authors) (2019) MHD natural convection of Cu–Al₂O₃ water hybrid nanofluids in a cavity equally divided into two parts by a vertical flexible partition membrane. *Journal of Thermal Analysis and Calorimetry*, 138 (2). pp. 1723-1743. ISSN 1388-6150

<https://doi.org/10.1007/s10973-019-08258-w>

© Akadémiai Kiadó, Budapest, Hungary 2019. This is an author produced version of a paper published in *Journal of Thermal Analysis and Calorimetry*. Uploaded in accordance with the publisher's self-archiving policy.

Reuse

Items deposited in White Rose Research Online are protected by copyright, with all rights reserved unless indicated otherwise. They may be downloaded and/or printed for private study, or other acts as permitted by national copyright laws. The publisher or other rights holders may allow further reproduction and re-use of the full text version. This is indicated by the licence information on the White Rose Research Online record for the item.

Takedown

If you consider content in White Rose Research Online to be in breach of UK law, please notify us by emailing eprints@whiterose.ac.uk including the URL of the record and the reason for the withdrawal request.



eprints@whiterose.ac.uk
<https://eprints.whiterose.ac.uk/>

**MHD natural convection of Cu-Al₂O₃ water hybrid nanofluids in a cavity equally divided
into two parts by a vertical flexible partition**

M. Ghalambaz^{*1}, S.A.M. Mehryan², E. Izadpanahi³, A. J. Chamkha^{4,5}, D. Wen^{1,6*}

¹School of Aeronautic Science and Engineering, Beihang University, Beijing, P.R.China

²Young Researchers and Elite Club, Yasooj Branch, Islamic Azad University, Yasooj, Iran

³Department of Mechanical and Materials Engineering, Florida International University, Miami, FL 33174, United States. E-mail: eizad001@fiu.edu

⁴Mechanical Engineering Department, Prince Mohammad Bin Fahd University, Al-Khobar 31952, Saudi Arabia

⁵Prince Sultan Endowment for Energy and Environment, Prince Mohammad Bin Fahd University, Al-Khobar 31952, Saudi Arabia, E-mail: achamkha@pmu.edu.sa

⁶School of Chemical and Process Engineering, University of Leeds, Leeds, U,K

PACS: 47.15.Rq Laminar flows in cavities, channels, ducts, and conduits; 44.25.+f Natural convection.

Abstract

The aim of the present study is to investigate the effects of a hybrid nanofluid in a square cavity which is divided into two equal parts by a vertical flexible partition in the presence of a magnetic field. A numerical method called the Galerkin finite element method is utilized to solve the governing equations. The effects of different parameters, namely the Rayleigh number and the Hartmann number as well as the effects of nanoparticles concentration and magnetic field orientation, on the flow and heat transfer fields for the cases of pure fluid, nanofluid and hybrid nanofluid are investigated. The results indicate that the streamline patterns change remarkably and the convective heat transfer augments with increasing values of the Rayleigh number. Additionally, the maximum stress imposed on the flexible partition resulting from the interaction of the the partition and pure fluid is more than those caused by the nanofluid and the hybrid nanofluid. Furthermore, the increase of the magnetic field strength decreases the fluid velocity in the cavity, which declines the fluid thermal mixing, resulting in a conduction dominant heat transfer regime.

Keywords: Alumina-Copper nanoparticles; Hybrid nanofluid; Magnetic field; Flexible partition; Natural convection.

Nomenclature

B_0	applied magnetic field
\mathbf{d}_s	partition displacement-vector
E	Young's modulus in dimensional form
E_τ	dimensionless elasticity modulus
\mathbf{F}_v	vector of body force

g	gravity constant vector
L	the size of square cavity
P	fluid pressure
Pr	Prandtl number
Ra	Rayleigh number in vector form
Ra	Rayleigh number
t	time
T	fluid temperature
x,y	Cartesian coordinates
u	velocity vector
w	velocity vector of the moving coordinates of the grids

Greek symbols

α	thermal diffusivity
β	thermal expansion coefficient
φ	volume fraction of nanoparticles
γ	angle of magnetic field orientation
σ	the tensor of stress in partition
τ	non-dimensional time
ν	the fluid kinematic viscosity
ν	Poisson's ratio of the partition
ρ	density
ρ_R	density ratio of the fluid and the partition

Subscripts

c	Cold
f	Fluid
h	Hot
hnp	Hybrid nanoparticles

hnf	Hybrid nanofluid
nf	Nanofluid
P	Partition
s	Solid
Superscripts	
*	Dimensional parameters

1. Introduction

When it comes to enclosures, natural convection is the most important mean of heat transfer. Enclosures have a variety of applications in engineering such as boilers, energy storage and conservation systems, solar collectors-receivers, nuclear reactor systems, food and metallurgical industries, fire control and chemical, etc. Comprehensive studies have been done in recent years in this field [1-5]. Although, in many industrial applications, natural convection is considered as a beneficial phenomenon, the phenomenon becomes undesirable in some cases. One of the ways to control that is by applying an external magnetic field for magneto hydro dynamic (MHD) flows [6-11]. Results obtained by Sathiyamoorthy and Chamkha [8] indicated that the magnetic field with inclined angle affected the flow field and heat transfer rates. Sheikholeslami and Ganji investigated natural convection heat transfer of ferrofluid Fe_3O_4 -water nanofluid with a point source external magnetic field. Their results indicated the reduction of heat transfer caused by the magnetic field. Additionally, the flow inside cavities could be controlled by inserting dividers [14-15].

By using dividers inside cavities, the flow field, and correspondingly the heat transfer rate, can be controlled. The cavities with partitions can be classified in three groups: (a) partially-divided cavities [16-18], (b) cavities with inclined partitions [19-21] and (c) cavities fully-divided

horizontally or vertically with partition/partitions [22-25]. Jamesahar et al. [24] and Mehryan et al. [25] conducted a numerical study on the heat transfer in a divided square cavity using a flexible membrane. Jamesahar et al. [24] reported that the presence of a flexible diagonal partition could enhance the heat transfer, while the deflection of the flexible partition could also affect the heat and flow patterns. It was reported by Mehryan et al. [25] that there was an optimum value of magnetic inclination angle to maximize the heat transfer in the partitioned cavity. Additionally, they [25] reported that the dimensionless average temperature could be increased by applying the magnetic field when the Rayleigh number was in a moderate range ($Ra=10^6-10^7$), especially under a magnetic field (Hartmann number $Ha \geq 50$). Xu et al. [26] studied the transient natural convection inside a differentially heated cavity, which was filled with water and separated by a solid partition without any deflection. Three categorized natural convection main stages were found, including an initial stage, a transitional stage and a steady state stage.

Fully-divided cavities with an impermeable divider have many interesting applications. For instance, thermal conductive partitions are used to divided a box containing electronic units, and a conductive metallic cover can be installed to separate a sensitive electronic equipment from the surrounding. Chemical species, in many cases, should be segregated from each other in a chemical reactor, but heat can be transferred between the species through partitions. These practical applications of fully-divided cavities have motivated researchers to investigate the effect of dividers and partitions on convective heat and mass transfer phenomena in cavity enclosures. An experimental study has been done by Tatsuo et al. [27] considering the effects of N multiple vertical partitions on natural convection in a rectangular enclosure. It was found that the Nusselt number decreased with the increase of the partition numbers.

The natural convection phenomena in a portioned cavity was investigated by Oztop et al. [28]. On each sub-cavity, combinations of water and air were considered. Additionally, the effects of the presence of a vertical partition on the flow and heat inside in an enclosure was investigated by Kahveci [29], with the partition heated by uniform heat flux. It was shown that the vertical partition had a considerable effect on natural convection when the two parts of the enclosure were filled with the same fluid.

Dispersion of nanometer-sized particles in base fluids is now known as nanofluids, which are now widely used in a variety of thermal systems to enhance the heat transfer characteristics. Even for a small volume fraction of nanoparticles, nanofluids have shown an extreme increase in their thermal conductivities. Fluids such as water, ethylene glycol, bio-fluids, polymer solutions, oils and other lubricants are usually considered as base fluids. Different types of nanoparticles including metallic particles (Cu, Al, Fe, Au, and Ag) and non-metallic particles (Al_2O_3 , CuO, Fe_3O_4 , TiO_2 , and SiC) have been utilized in experimental and numerical studies. The non-metallic particles such as Al_2O_3 are known for their excellent stability and chemical inertness. Unfortunately, non-metallic particles show lower thermal conductivity compared to the metallic nanoparticles. Kahveci [30] investigated five types of nanoparticles inside a differentially heated, tilted enclosure, and showed that the average heat transfer rate of metallic nanoparticles was higher than those of non-metallic nanoparticles. On the other hand, metallic nanoparticles, for instance, copper (Cu) or aluminum (Al) have much higher thermal conductivities, but their poor stability and tendency to chemical reactions prevented researchers to utilize them widely.

Most of the earlier investigations have addressed the effect of using a single type of metallic or non-metallic nanoparticles on the heat transfer performance of nanofluids. However, combination of non-metallic nanoparticles with a small amount of metal nanoparticles can enhance

the thermal properties of the base fluid significantly. Jeena et al. [31] have successfully synthesized a homogeneous mixture of well dispersed CuO and Al₂O₃ composite briquette by using hydrogen reduction technique. Suresh et al. [32] have investigated the thermos-physical properties of Alumina-Copper hybrid nanofluids. The outcomes demonstrated that the presence of hybrid nanoparticles significantly enhanced the the thermal conductivity and dynamic viscosity of hybrid nanofluids. In an experimental study by Suresh et al. [33], it was reported that the Nusselt number can be increased up to 13.56% by using Al₂O₃-Cu hybrid nanofluids. Hemmat et al. [34] prepared a sample of Ag-MgO/water hybrid nanofluids and studied the thermal conductivity and dynamic viscosity of the hybrid nanofluids for various volume fractions of nanoparticles up to 2%. They compared the results with different existing empirical and theoretical correlations. Moghadassi et al. [35] theoretically investigated laminar forced-convection heat transfer of single water-based Al₂O₃ nanofluids and hybrid Al₂O₃-Cu nanofluids up to 0.1% volume fraction of nanoparticles.

As mentioned, in very recent studies, Jamesahar et al. [24] and Mehryan et al. [25] have studied the heat transfer of a pure fluid in a square cavity divided into two sub-cavities by a flexible partition. Following [24] and [25], the present study aims to analyze the effects of Cu-Al₂O₃/water hybrid nanofluid and magnetic field on the natural convection inside a fully-divided cavity. The motivation of the present study is to answer the following questions:

- 1- What is the effect of magnetic field inclination on the heat and flow patterns of hybrid nanofluids?
- 2- Does the presence of nanoparticles enhances the heat transfer in the divided cavity? Is there any significant difference between heat transfer enhancement of Al₂O₃ nanoparticles and Cu-Al₂O₃ hybrid nanoparticles?

3-How the presence of nanoparticles could change the shape of the flexible partition and the heat transfer rate?

4- Which types of nanoparticles (Al_2O_3 or $\text{Cu-Al}_2\text{O}_3$) are better for heat transfer enhancement in the presence of a magnetic field?

2. Description of the work

A view of the considered problem geometry is shown schematically in Fig. 1 which is utilized to derive the governing equations and boundary conditions. The dimensions of the enclosure in x^* , y^* coordinates are so much higher than that in z^* one. Accordingly, a two dimensional mathematical domain is considered. It is defined that the left surface with the temperature of T_h is hotter than the right surface with the temperature of T_c ($T_h > T_c$). The lower and upper bounds of the enclosure are thermally impervious. Moreover, it is assumed that all the solid boundaries are made of electrically non-conducting material. A vertical thin flexible partition breaks up the square cavity into two equal parts. t_p^* represents the thickness of the flexible partition. The flexible partition material is isotropic and nonmagnetic. Both parts are glutted with a Newtonian electromagnetic hybrid nanofluid $\text{Cu-Al}_2\text{O}_3/\text{water}$ or nanofluid $\text{Al}_2\text{O}_3/\text{water}$. A hybrid nanofluid contains a base fluid and two or more types of nanoparticles. In this study, solid particles of hybrid nanofluid are the nanoparticles of Al_2O_3 and Cu . The thermophysical properties of the forming components of hybrid/ regular nanofluid are represented in Table 1. Both the types of nanoparticles are always suspended and stable. This means that the nanoparticles do not agglomerate and become collective. There is a thermal and dynamic equilibrium between the suspended nanocomposite particles and the host fluid. The fluid flow is laminar and steady state. The buoyancy effects are modeled using Boussinesq approximation. Since the flexible partition is

thin and with low thermal resistance, the gradient of temperature in it is zero. Additionally, all the solid surfaces are impervious to the mass flow. The flow domain is exposed a tilted magnetic field with the amplitude and angle of B_0 and γ , respectively. It is supposed that the convection and diffusion values of the energy balance are so much higher than viscous dissipation and Joule heating. The densities of the hybrid nanofluid and the flexible partition are the same. The partition behaves such a hyper-elastic material reacting nonlinearly against applied loads.

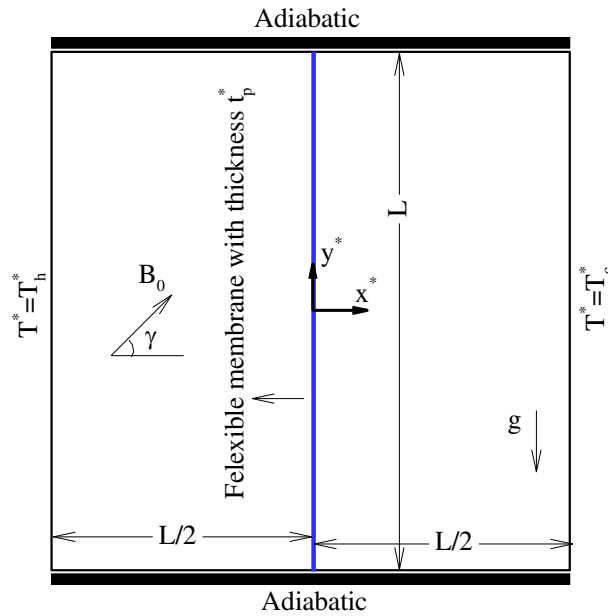


Fig. 1. The schematic view of the physical model and boundary conditions

The Lorentz force is one that is applied to the flow domain due to the existence of the magnetic field vector \mathbf{B} with the density of electrical current \mathbf{J} :

$$\mathbf{F} = \mathbf{J} \times \mathbf{B} \quad (1a)$$

where \mathbf{J} is defined by Ohm's law:

$$\mathbf{J} = \sigma_{\text{hnf}} (-\nabla\phi + \mathbf{u}^* \times \mathbf{B}) \quad (1b)$$

where σ_{hnf} represents the electrical conductivity of the fluid. \mathbf{u}^* (u^*, v^*) is the velocity vector of the fluid in the cavity. The bounds of the enclosure are electrically impervious, so, according to the Maxwell theory $\nabla\phi = 0$. Therefore, we have

$$\mathbf{F} = \sigma_{\text{hnf}} (\mathbf{u}^* \times \mathbf{B}) \times \mathbf{B} \quad (1c)$$

Table 1. The thermophysical properties of the hybrid nanofluid components [36-37]

Physical properties	water	Cu	Al ₂ O ₃
c_p (J/kg. K)	4179	385	765
k (W/m. K)	0.613	401	40
α (m ² /s)	1.47×10^{-7}	1.11×10^{-4}	131.7×10^{-7}
β (K ⁻¹)	21×10^{-5}	1.67×10^{-5}	0.85×10^{-5}
ρ (kg/m ³)	997.1	8933	3970
μ (kg/m. s)	8.9×10^{-4}	-	-
σ (W m ⁻¹ K ⁻¹)	0.05	5.96×10^7	1×10^{-10}

Description of the reciprocal effects of the fluid and deformable solid material is performed by the known technique of the Arbitrary Lagrangian-Eulerian (ALE). The fluid flow within the enclosure is portrayed by the incompressible mass conservation and the linear momentum equations for the pressure and velocity fields:

$$\nabla^* \cdot \mathbf{u}^* = 0 \quad (2)$$

$$\frac{\partial \mathbf{u}^*}{\partial t} + (\mathbf{u}^* - \mathbf{w}^*) \cdot \nabla^* \mathbf{u}^* = -\frac{1}{\rho_{\text{hnf}}} \nabla^* P^* + \frac{\mu_{\text{hnf}}}{\rho_{\text{hnf}}} \nabla^{*2} \mathbf{u}^* + \frac{\sigma_{\text{hnf}}}{\rho_{\text{hnf}}} (\mathbf{u}^* \times \mathbf{B}) \times \mathbf{B} + \beta_{\text{hnf}} \mathbf{g} (T^* - T_c^*) \quad (3)$$

$$\frac{\partial T^*}{\partial t} + (\mathbf{u}^* - \mathbf{w}^*) \cdot \nabla^* T^* = \alpha_{\text{hnf}} \nabla^{*2} T^* \quad (4)$$

The structural deformations of the flexible partition can be achieved by the following nonlinear geometric and elastic formulation:

$$\rho_s \frac{d^2 \mathbf{d}_s^*}{dt^2} - \nabla^* \boldsymbol{\sigma}^* = \mathbf{F}_v^* \quad (4)$$

\mathbf{F}_v^* of the above-written equation is the applied volume forces on the deformable partition, $\boldsymbol{\sigma}^*$ is the solid stress tensor, \mathbf{d}_s^* the displacement vector of moving coordinate system so that $d\mathbf{d}_s^*/dt = \mathbf{w}^*$ and ρ_s is the density of the partition.

In this study, the stress tensor $\boldsymbol{\sigma}^*$ is computed using a Neo-Hookean model to characterize the stress-strain nonlinear behavior of a hyper-elastic material with large deformations. The hyper-elastic theory is used more for modeling of rubbery behavior of a polymeric material and polymeric foams that can have large deformations. The model can be written as follows:

$$\boldsymbol{\sigma}^* = J^{-1} \mathbf{F} \mathbf{S} \mathbf{F}^T \quad (5)$$

where

$$\mathbf{F} = (\mathbf{I} + \nabla^* \mathbf{d}_s^*), \quad J = \det(\mathbf{F}) \quad \text{and} \quad \mathbf{S} = \partial \mathbf{W}_s / \partial \boldsymbol{\varepsilon} \quad (6)$$

are the deformation gradient, determinant of the matrix \mathbf{F} and the partial differential of the density function of strain energy, respectively. Also, the density function of the strain energy \mathbf{W}_s and strain $\boldsymbol{\varepsilon}$ is defined through the equations below:

$$\mathbf{W}_s = \frac{1}{2} \mu_1 (J^{-1} \mathbf{I}_1 - 3) - \mu_1 \ln(J) + \frac{1}{2} \lambda (\ln(J))^2 \quad (7)$$

$$\boldsymbol{\varepsilon} = \frac{1}{2} (\nabla^* \mathbf{d}_s^* + \nabla^{*\top} \mathbf{d}_s^{*\top} + \nabla^* \mathbf{d}_s^{*\top} \nabla^* \mathbf{d}_s^*) \quad (8)$$

where

$$\lambda = E\nu / ((1+\nu)(1-2\nu)) \quad \mu = E / (2(1+\nu)) \quad (9)$$

λ and μ of the above equations, known as Lamé's first and second constants, respectively, is related to poisson coefficient and elasticity module using $\mu = E / (2(1+\nu))$, and $\lambda = E\nu / ((1+\nu)(1-2\nu))$. I_1 is called the first constant of the deformation tensor.

All the bounds of the enclosure are motionless ($u^* = v^* = 0$). The lower and topper bounds of the both sub-cavities are thermally insulated ($\partial T^* / \partial y^* = 0$). The right hand wall is at the low temperature $T^* = T^*_c$, while the temperature of the opposite wall is higher $T^* = T^*_h$.

Along the fluid-solid interface, continuity of the dynamic motion and kinematic forces are the boundary conditions utilized to model the fluid and deformable divider interaction. These conditions can be represented as

$$\frac{\partial \mathbf{d}_s^*}{\partial t} = \mathbf{u}^* \quad \text{and} \quad \boldsymbol{\sigma}^* \cdot \mathbf{n} = -P^* + \mu_f \nabla^* \mathbf{u}^* \quad (8)$$

Applying the conservation of energy on the flexible divider along with the previously assumptions results in the equation below:

$$\frac{\partial T^{*+}}{\partial n} = \frac{\partial T^{*-}}{\partial n} \quad \text{and} \quad T^{*+} = T^{*-} \quad (12)$$

In this equation, the plus and minus marks denote the right and left sides of the deformable divider, respectively. Also, the boundary condition for both eyelets can be represented as follows:

$$\left[-P^* + \mu_{\text{hmf}} \nabla^* \mathbf{u}^* \right] \cdot \mathbf{n} = 0 \quad (13)$$

To provide with dimensions, non-dimensional parameters are introduced below;

$$\mathbf{d}_s = \frac{\mathbf{d}_s^*}{L}, \quad \boldsymbol{\sigma} = \frac{\boldsymbol{\sigma}^*}{E}, \quad \tau = \frac{t\alpha_f}{L^2}, \quad (x, y) = \frac{(x^*, y^*)}{L}, \quad (14a)$$

$$\mathbf{u} = \frac{\mathbf{u}^*L}{\alpha_f}, \quad \mathbf{w} = \frac{\mathbf{w}^*L}{\alpha_f}, \quad P = \frac{L^2}{\rho_f \alpha_f^2} P^*, \quad T = \frac{T_h^* - T_c^*}{T_h^* - T_c^*} \quad (14b)$$

$$\nabla = \frac{\nabla^*}{1/L}, \quad \nabla^2 = \frac{\nabla^{*2}}{1/L^2}, \quad t_p = \frac{t^*}{L} \quad (14c)$$

To dimensionalize the equations, the above parameters are substituted for the Eqs. (1)-(4). Therefore, we then have,

$$\frac{1}{\rho_R} \frac{d^2 \mathbf{d}_s}{d\tau^2} - E_\tau \nabla \boldsymbol{\sigma} = E_\tau \mathbf{F}_v \quad (15)$$

$$\nabla \cdot \mathbf{u} = 0 \quad (16)$$

$$\begin{aligned} \frac{\partial \mathbf{u}}{\partial \tau} + (\mathbf{u} - \mathbf{w}) \cdot \nabla \mathbf{u} = & -\frac{\rho_f}{\rho_{hnf}} \nabla P + \left(\frac{\rho_f}{\rho_{hnf}} \right) \left(\frac{\mu_{hnf}}{\mu_f} \right) \text{Pr} \nabla^2 \mathbf{u} + \frac{(\rho\beta)_{hnf}}{\rho_{hnf} \beta_f} \text{Pr} \text{Ra} T \\ & + \left(\frac{\rho_f}{\rho_{hnf}} \right) \left(\frac{\sigma_{hnf}}{\sigma_f} \right) \text{Pr} (\mathbf{u} \times \mathbf{Ha}) \times \mathbf{Ha} \end{aligned} \quad (17)$$

$$\frac{\partial T}{\partial \tau} + (\mathbf{u} - \mathbf{w}) \cdot \nabla T = \frac{\alpha_{hnf}}{\alpha_f} \nabla^2 T \quad (18)$$

In Eq. (13), ρ_R is the density ratio, E_τ is the dimensionless elasticity modulus and \mathbf{F}_v is dimensionless volume force vector.

$$\rho_R = \frac{\rho_{hnf}}{\rho_s}, \quad E_\tau = \frac{EL^2}{\rho_{hnf} \alpha_f^2}, \quad \mathbf{F}_v = \frac{(\rho_{hnf} - \rho_s) \mathbf{L}g}{E} \quad (19)$$

In Eq. (15), the dimensionless numbers

$$\text{Pr} = \frac{\nu_f}{\alpha_f}, \text{Ra} = \frac{g\beta(T_h - T_c)L^3}{\nu_f \alpha_f}, \mathbf{Ha} = \mathbf{LB} \sqrt{\frac{\sigma_f}{\mu_f}} \quad (20)$$

The non-dimensional parameter of Hartmann number is a vector with two components along the x- ($\text{Ha} \sin(\gamma)$) and the y-axes ($\text{Ha} \cos(\gamma)$). The volume force expression rising from the magnetic field, known as Lorentz force, is rewritten as follows:

In the x-direction:

$$\left(\frac{\rho_f}{\rho_{\text{hnf}}} \right) \left(\frac{\sigma_{\text{hnf}}}{\sigma_f} \right) \text{Pr Ha}^2 (v \sin \gamma \cos \gamma - u \sin^2 \gamma) \quad (21)$$

In the y-direction:

$$\left(\frac{\rho_f}{\rho_{\text{hnf}}} \right) \left(\frac{\sigma_{\text{hnf}}}{\sigma_f} \right) \text{Pr Ha}^2 (u \sin \gamma \cos \gamma - v \cos^2 \gamma) \quad (22)$$

where

$$\rho_{\text{hnf}} = \rho_f (1 - \varphi_{\text{hnf}}) + \rho_{\text{Al}_2\text{O}_3} \varphi_{\text{Al}_2\text{O}_3} + \rho_{\text{Cu}} \varphi_{\text{Cu}} \quad (23)$$

$$(\rho\beta)_{\text{hnf}} = (1 - \varphi_{\text{hnf}})(\rho\beta)_f + \varphi_{\text{Al}_2\text{O}_3} (\rho\beta)_{\text{Al}_2\text{O}_3} + \varphi_{\text{Cu}} (\rho\beta)_{\text{Cu}} \quad (24)$$

$$\sigma_{\text{hnf}} = \sigma_f \left(1 + \frac{3 \left(\frac{\sigma_{\text{hnf}}}{\sigma_f} - 1 \right) \varphi_{\text{hnf}}}{\left(\frac{\sigma_{\text{hnf}}}{\sigma_f} + 2 \right) - \left(\frac{\sigma_{\text{hnf}}}{\sigma_f} - 1 \right) \varphi_{\text{hnf}}} \right) \quad (25)$$

$$\begin{aligned}\varphi_{\text{hnp}} &= \varphi_{\text{Al}_2\text{O}_3} + \varphi_{\text{Cu}} \\ \sigma_{\text{hnp}} \varphi_{\text{hnp}} &= \sigma_{\text{Al}_2\text{O}_3} \varphi_{\text{Al}_2\text{O}_3} + \sigma_{\text{Cu}} \varphi_{\text{Cu}}\end{aligned}\tag{26}$$

In all the above-mentioned relations, φ represents the nanoparticles concentration. here $\rho_s = \rho_{\text{hnf}}$, therefore the volume force of F_v is zero. Noticing the thermophysical properties represented in Table 1, the electrical conductivity orders of Al_2O_3 and Cu nanoparticles are $O(10^{-10})$ and $O(10^7)$, respectively. Hence, compared to the nanoparticles of Cu, the electrical conductivity of Al_2O_3 nanoparticles is very close to zero. Therefore, the electrical conductivity of the hybrid nanoparticles can be rewritten as follows:

$$\sigma_{\text{hnp}} = \left(\frac{\varphi_{\text{Cu}}}{\varphi_{\text{hnp}}} \right) \sigma_{\text{Cu}}\tag{27}$$

The heat capacity of the hybrid nanofluid is calculated from the following equation:

$$(\rho c_p)_{\text{hnf}} = (1 - \varphi_{\text{hnp}})(\rho c_p)_f + \varphi_{\text{Al}_2\text{O}_3} (\rho c_p)_{\text{Al}_2\text{O}_3} + \varphi_{\text{Cu}} (\rho c_p)_{\text{Cu}}\tag{28}$$

In addition, by employing the the classical Maxwell [39] and Bruggeman [40] models, we then have:

The classical Maxwell model [39]:

$$\frac{k_{\text{hnf}}}{k_f} = \frac{k_{\text{hnp}} + 2k_f - 2\varphi_{\text{hnp}}(k_f - k_{\text{hnp}})}{k_{\text{hnp}} + 2k_f + \varphi_{\text{hnp}}(k_f - k_{\text{hnp}})}\tag{29}$$

The classical Bruggeman model [40]:

$$k_{\text{hnf}} = \frac{1}{4} \left[(3\varphi_{\text{hnp}} - 1)k_{\text{hnp}} + (2 - 3\varphi_{\text{hnp}})k_f \right] + \frac{k_f}{4} \sqrt{\Delta} \quad (30)$$

$$\Delta = \left[(3\varphi_{\text{hnp}} - 1)^2 \left(\frac{k_{\text{hnp}}}{k_f} \right) + (2 - 3\varphi_{\text{hnp}})^2 + 2(2 + 9\varphi_{\text{hnp}} - 9\varphi_{\text{hnp}}^2) \left(\frac{k_{\text{hnp}}}{k_f} \right) \right] \quad (31)$$

where in both of the above relations k_{hnp} is defined as

$$k_{\text{hnp}} \varphi_{\text{hnp}} = k_{\text{Al}_2\text{O}_3} \varphi_{\text{Al}_2\text{O}_3} + k_{\text{Cu}} \varphi_{\text{Cu}} \quad (32)$$

In order to check the validity of these relations for the hybrid nanofluid Cu-Al₂O₃/ water, the values of the thermal conductivity obtained from both of the above relations for the hybrid nanofluid is calculated for different volume concentrations. Then these values have been evaluated using the experimental data as are shown in Fig. 2. (a) This comparison clearly depicts that the Maxwell and Bruggman relations can not estimate the real values of the thermal conductivity of the hybrid nanofluid of Cu-Al₂O₃/ water. Therefore, the remaining calculations are done based on the experimental thermal conductivity. Also, a comparison is done between the theoretical models and the experimental results to study the potential of the classical models to estimate the viscosity of the hybrid nanofluid Cu-Al₂O₃/ water. Three models are used as follows:

Einstein model [41]:

$$\frac{\mu_{\text{hnf}}}{\mu_f} = 1 + k_{\mu} \varphi_{\text{hnp}} \quad (33)$$

Brinkman model [42]:

$$\frac{\mu_{\text{hnf}}}{\mu_f} = \frac{1}{(1 - \varphi_{\text{hnp}})^{2.5}} \quad (34)$$

Batchelor model [43]:

$$\frac{\mu_{\text{hnf}}}{\mu_f} = 1 + k_{\mu 1} \phi_{\text{hnp}} + k_{\mu 2} \phi_{\text{hnp}}^2 \quad (35)$$

As this comparison shows in Fig. 2 (b), the classical models significantly underpredict the viscosity. For this reason, the experimental results are employed to continue the computations. The experimental thermal conductivity and dynamic viscosity of the nanofluid Al₂O₃-water and Cu-Al₂O₃/ water hybrid nanofluid are given in Table 2. Table 2 also shows the volume fractions of both the nanoparticles Cu and Al₂O₃ suspended in the nanofluid.

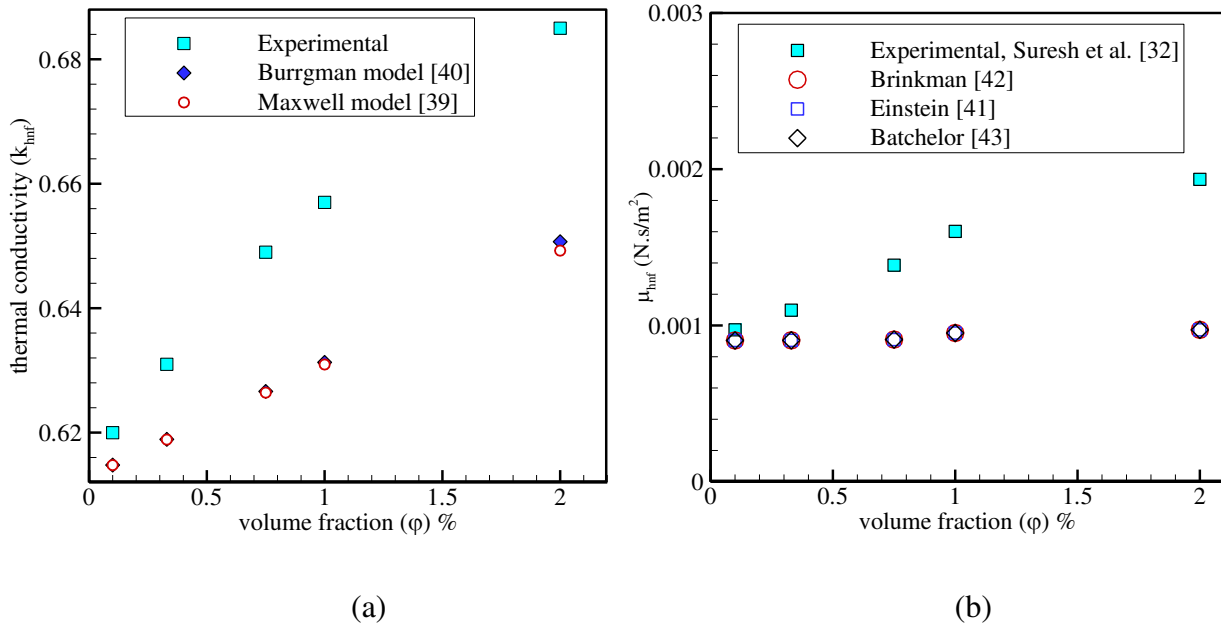


Fig. 2. (a): Thermal conductivity, (b): dynamic viscosity obtained by the classical models.

Table 2. The thermal conductivity and dynamic viscosity obtained by experiment [32]

ϕ_{hnp} (%)	ϕ_{Cu} (%)	$\phi_{\text{Al}_2\text{O}_3}$ (%)	k (W/m·K)	μ × 10 ³ (kg/m.s)
0.1	0.0038	0.0962	0.619982	0.972

0.33	0.0125	0.3175	0.63098	1.098
0.75	0.0285	0.7215	0.649004	1.386
1	0.038	0.962	0.657008	1.602
2	0.0759	1.9241	0.684992	1.935
0.1	0	0.1	0.614055	0.9041
0.33	0	0.33	0.6190041	0.9049
0.75	0	0.75	0.6309797	0.9098
1	0	1	0.6437496	0.95184
2	0	2	0.6571916	0.972

The dimensionless forms of the boundary conditions are:

For all the out bounds $u = v = 0$

For the adiabatic walls at the top and bottom $\frac{\partial T}{\partial y} = 0$ (36a)

For the left bound $T = 1$

For the right bound $T = 0$ (36b)

For the partition $\frac{\partial T^+}{\partial n} = \frac{\partial T^-}{\partial n}$ and $T^+ = T^-$ (36c)

On the solid-fluid interface:

$$\frac{\partial \mathbf{d}_s}{\partial \tau} = \mathbf{u} \text{ and } E_r \boldsymbol{\sigma} \cdot \mathbf{n} = -P + \left(\frac{\mu_{\text{hnf}}}{\mu_f} \right) \text{Pr} \nabla \mathbf{u} \quad (37)$$

For the eyelets:

$$\left[-P + \left(\frac{\mu_{\text{hnf}}}{\mu_f} \right) \text{Pr} \nabla \mathbf{u} \right] \cdot \mathbf{n} = 0 \quad (38)$$

The local heat transfer rate is defined by the following relation:

$$\text{Nu}_{\text{local}} = -\frac{k_{\text{hnf}}}{k_f} \frac{\partial T}{\partial x} \quad (39)$$

Integrating the above relation leads to the mean Nusselt number:

$$\text{Nu}_{\text{avg}} = \int_0^1 \text{Nu}_{\text{local}} dy \quad (40)$$

Another important parameter is the mean temperature of the whole domain:

$$T_{\text{avg}} = \frac{\int_A T_{\text{local}} dA}{\int_A dA} \quad (41)$$

3. Solution procedure, grid evaluation and verification

Since the system of the governing equations (15)-(18) as well as the boundary conditions (36)-(38) are coupled and nonlinear, it is necessary to use a numerical method to solve them. To do this, the numerical Galerkin finite element approach is applied to do the weak form of the equations in the deformable grid system of ALE. The details of the Galerkin finite element approach have been explained in [44]. Fluid and solid are two regions of the computational domain. Both the regions are discretized to small structural elements. Before starting calculations, to evaluate the solution sensitivity to the element numbers, the grid independence test is done. The grid used is non-uniform structural quadrilateral grid. This test is performed for the case $\text{Ra}=10^8$, $\text{Ha}=0$, $\varphi_{\text{hnf}}=0$ and $E_\tau=10^{14}$. The results of the examination are presented in Fig. 3 and Table 3. The figure and table are made based on Nu_{local} and ψ_{max} , respectively. ψ is the stream function. Fig. 3 shows that the variations of Nu_{local} are so slight when the number of elements is more than 50×50 . However, as it is shown in Table 3, the relative error is 15.40 % for this grid. So, it is necessary to

evaluate the grids with the more number of elements. The elements rising process continues until the relative error becomes less than 1 % (exactly 0.58 %) in the grid 130×130. Therefore, the grid 130×130 is considered very appropriate and is chosen.

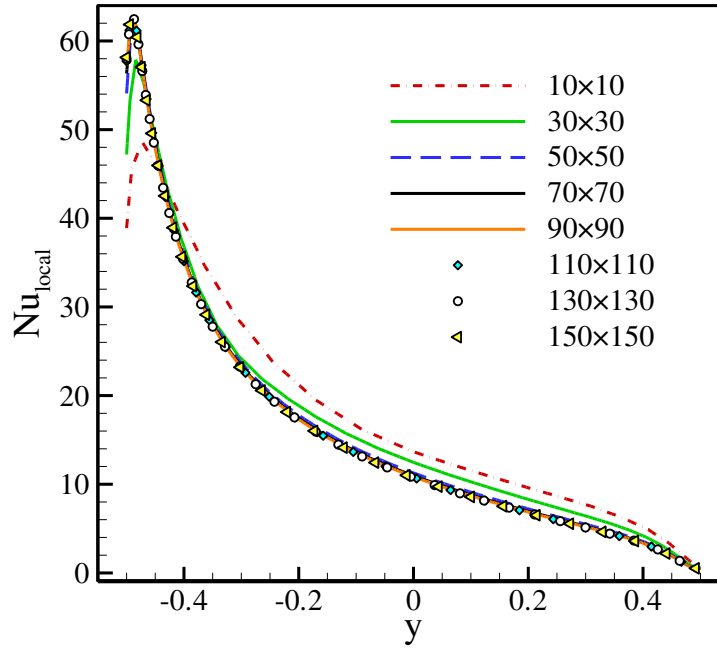


Fig. 3. Grid independence test in $Ra=10^8$, $\phi_{hnp}=0$ and $Ha=0$

Table 3. The grid independence test base on the maximum value of streamline

Elements	10×10	30×30	50×50	70×70	90×90	110×110	130×130	150×150
$ \psi _{\max}$	64.05	52.68	44.57	42.35	41.51	41.08	40.85	40.70
*Error		17.75	15.40	4.98	1.99	1.02	0.58	0.36

* Error = $100 \times (|\psi|_{\max} \text{ in Previous grid size} - |\psi|_{\max} \text{ in the present grid size}) / |\psi|_{\max} \text{ in Previous grid size}$

In the current investigation, several comparisons are performed to confirm the correctness and precision of the used numerical approach. The first validation consists of the case investigated in [30]. This comparison is shown in Fig. 4. The very high accordance between the results

published by [30] and those obtained by the present study vouches the correctness and precision of the numerical approach.

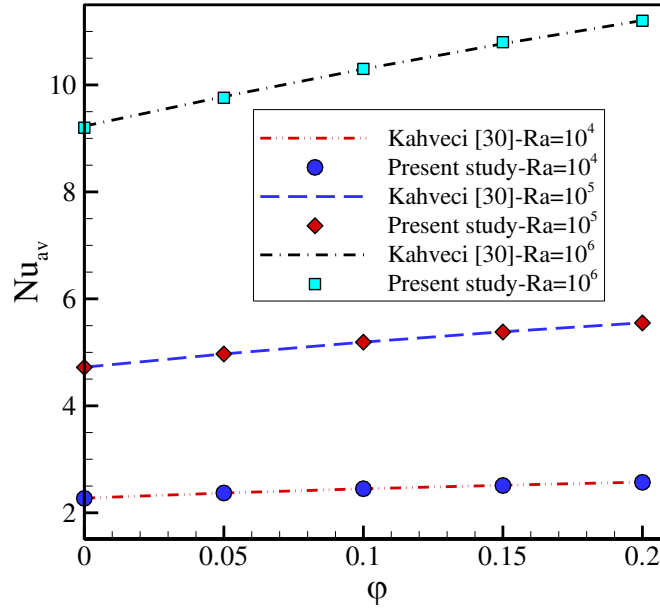


Fig. 4. Variation of Nu_{avg} according to nanoparticles concentration ϕ at the various values of Ra resulted from [30] and the present study

In the second validation (shown in Fig. 5), the curvature of the lower bound in the lid-driven cavity modeled by the present study and Küttler and Wall [45] are compared. The deformation curves simulated in this study and literature [45] are in good agreement. Therefore, we can claim that the numerical procedure used is absolutely true.

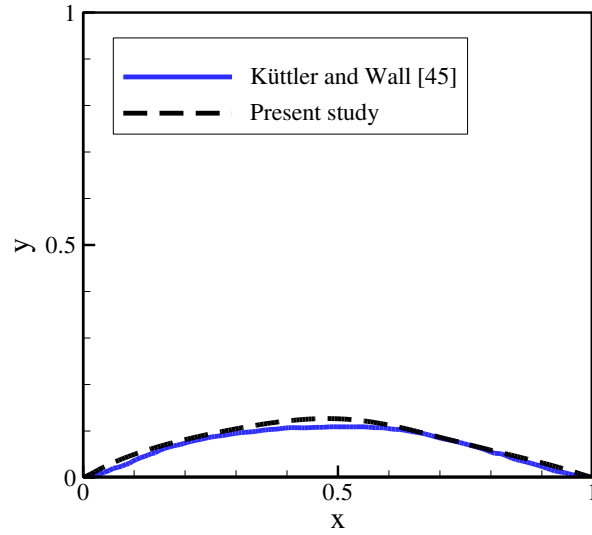


Fig. 5. The deformation curves of the deformable lower bound of the lid-driven enclosure examined by Küttler and Wall [45] and the present study at $t=7.5s$

The third validation is presented in Fig. 6 and shows the isotherms contours simulated in the current investigation and Sathiyamoorthy and Chamkha [8]. The good agreement between the outcomes of this investigation and those of Sathiyamoorthy and Chamkha [8] states that the solution method employed can correctly simulate a cavity under an external volume force.

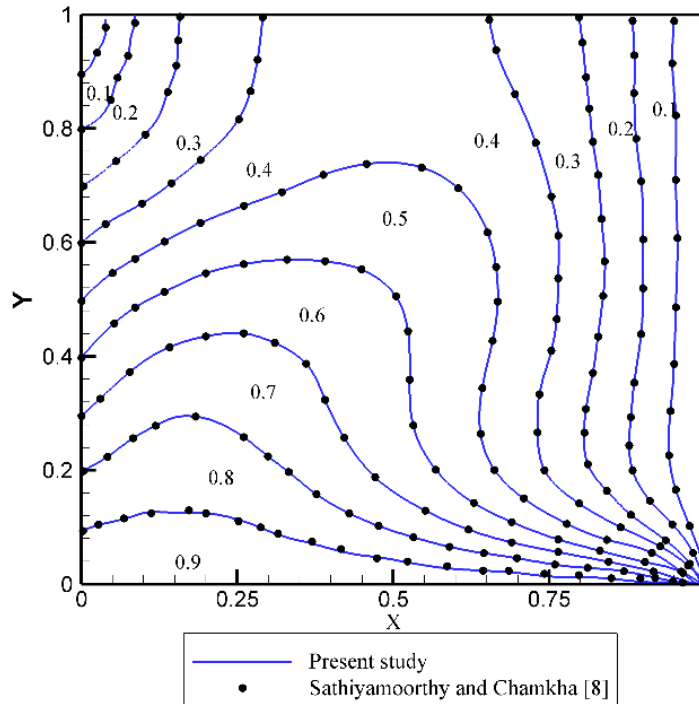


Fig. 6. The isotherms of this study and those obtained by Sathiyamoorthy and Chamkha [8] for the case of a simple cavity when $Ha = 50$, $Ra = 10^5$, $Pr = 0.025$ and $\gamma = 0$

As shown in Fig. 7, there exist an excellent compatibility for the numerical results rising from the current survey, experimental data of literature [27] and Churchill's equation [46]. Therefore, the used code is trusty. N is the vertical partitions dividing the enclosure. AR is the ratio of the height to width of the enclosure.

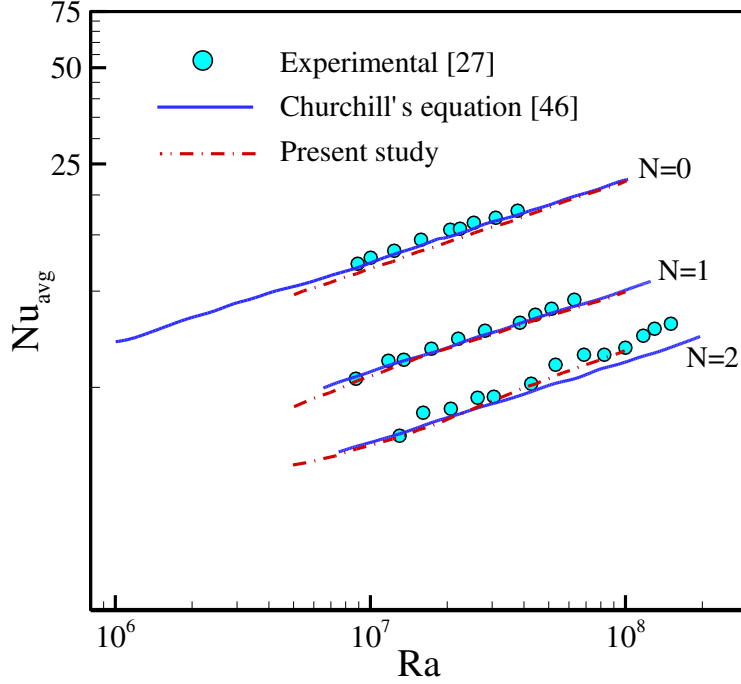


Fig. 7. The comparison of the results obtained by the present study with experimental dates [27] and Churchill's relation [46] at $Pr=6$ and $AR=4$

In the last validation, the precision and correctness of our data have been measured with those of Xu et al. [26]. These authors have studied the transient natural convection in a partitioned cavity subject to temperature difference at the side walls. Considering a very rigid partition and assuming zero fraction of nanoparticles, the results of the present study can be compared with the results reported in [26]. Fig. 8 depicts a comparison between the results of the present study and [26] for the transient non-dimensional temperature profile. The non-dimensional temperature profile of Fig. 8 corresponds to a specified point with the coordinate of (0.0083, 0.375) which is located next to the partition. It is worth noticing that Xu et al. [26] have used $\tau = t\alpha Ra^{1/2}/L^2$ as the non-dimensional time variable.

the definition of the dimensionless time in the present investigation and Xu et al. [26] is different. The dimensionless time and Rayleigh number are defined as $\tau = t\alpha_f Ra^2/L^2$ and

$\mathbf{Ra} = \mathbf{g}\beta(T_h^* - T_c^*)L^3 / \nu_f \alpha_f$ in the study of Xu et al. [26]. As can be seen from Fig. 8, there is an excellent agreement between the outcomes of this work and those reported in [26]. This validation verifies the sufficiency of the present formulation and solution to simulate the transient natural convection in the fluid domain and the partition.

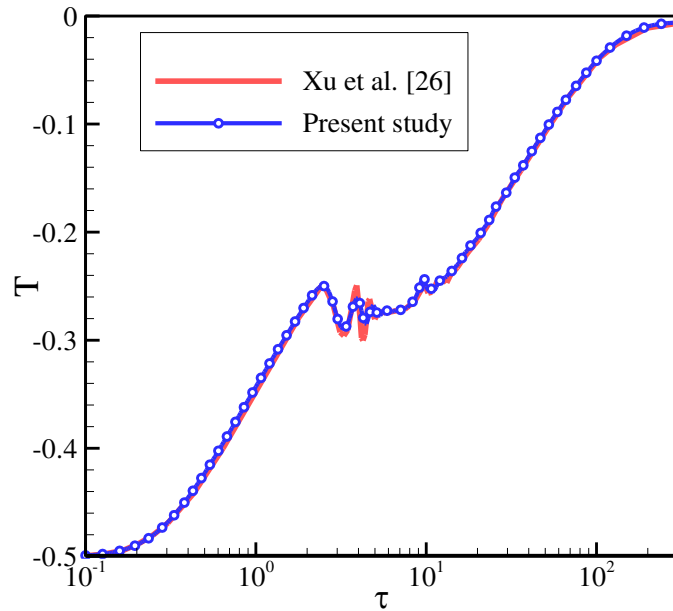


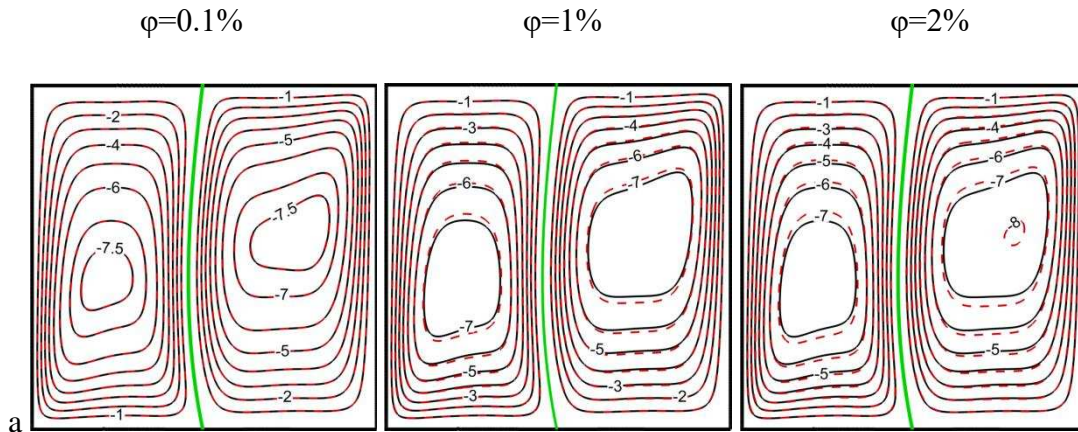
Fig. 8. Comparison of the dimensionless temperature reported by Xu et al. [26] and this study at the certain point (0.0083, 0.375)

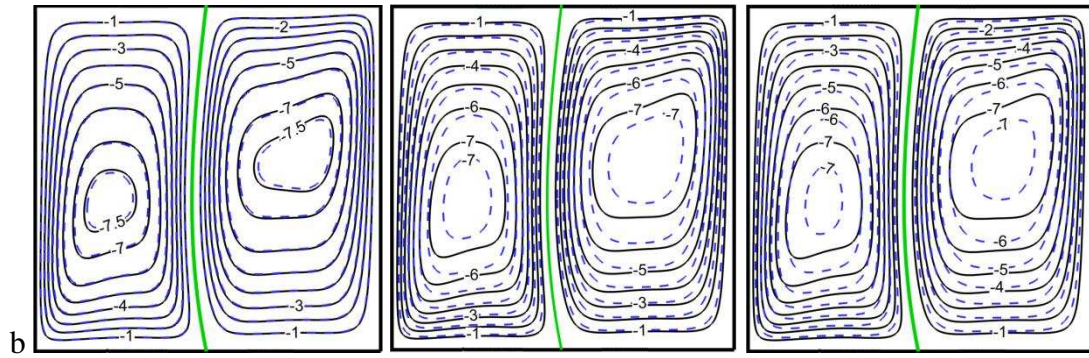
Results and discussion

This section deals with the results acquired from the problem simulation. Here, the impacts of the dimensionless parameters like the Rayleigh number ($10^6 \leq Ra \leq 10^8$), nanoparticles concentration ($0.0 \leq \varphi \leq 0.02$), Hartmann number ($0.0 \leq Ha \leq 200$) and the angle of magnetic-field vector ($0 \leq \gamma \leq \pi$) on the flow and temperature fields are investigated. Additionally, the effects of these parameters on the stresses of the flexible partition are studied. The values of $E_r=10^{14}$ and

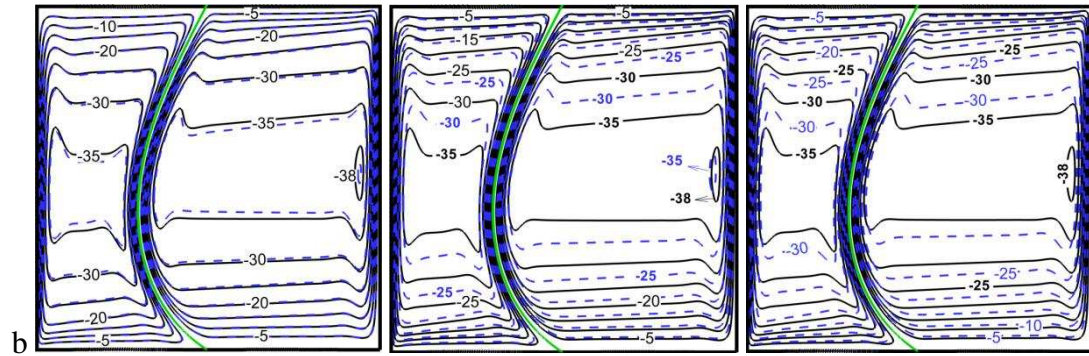
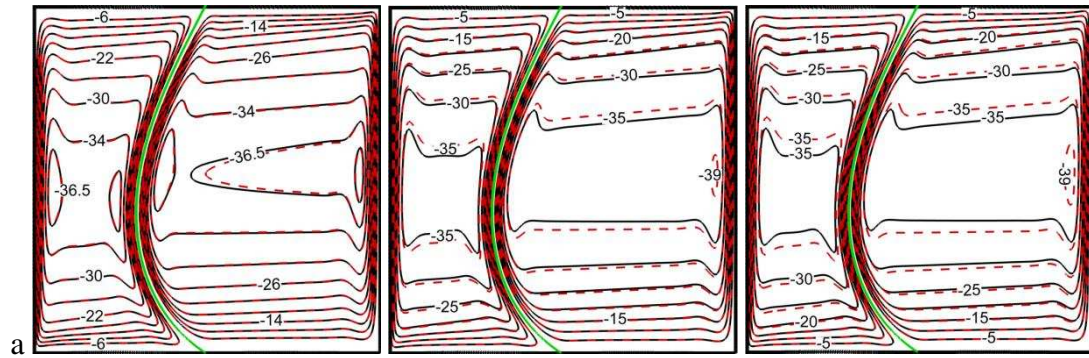
$Pr=6.2$ are kept constant. As previously mentioned, the densities of the hybrid nanofluid and the flexible partition are the same. Therefore, ρ_R and F_v have always the value of 1 and 0, respectively. The angles rang of the magnetic field vector has been selected from 0 to π because the Lorentz force is a periodic one with the period of π .

Fig. 9 depicts the streamlines for different values of nanoparticles concentration at low Rayleigh number 10^6 and high Rayleigh number 10^8 . Here, Ha is 50 and γ is $2\pi/3$. Solid and dashed lines have been defined for pure fluid and nanofluid, respectively. For both low and high Rayleigh number 10^6 and 10^8 , the results illustrate that the presence of the Al_2O_3 nanoparticles enhances the strength of fluid flow while the simultaneous presence of Cu and Al_2O_3 nanoparticles reduces the flow strength. Moreover, it is observed that the governing streamlines patterns do not change by the presence of Cu- Al_2O_3 and Al_2O_3 nanoparticles; however, the nanoparticles can change the initial location of the streamlines.





(I): $Ra=10^6$

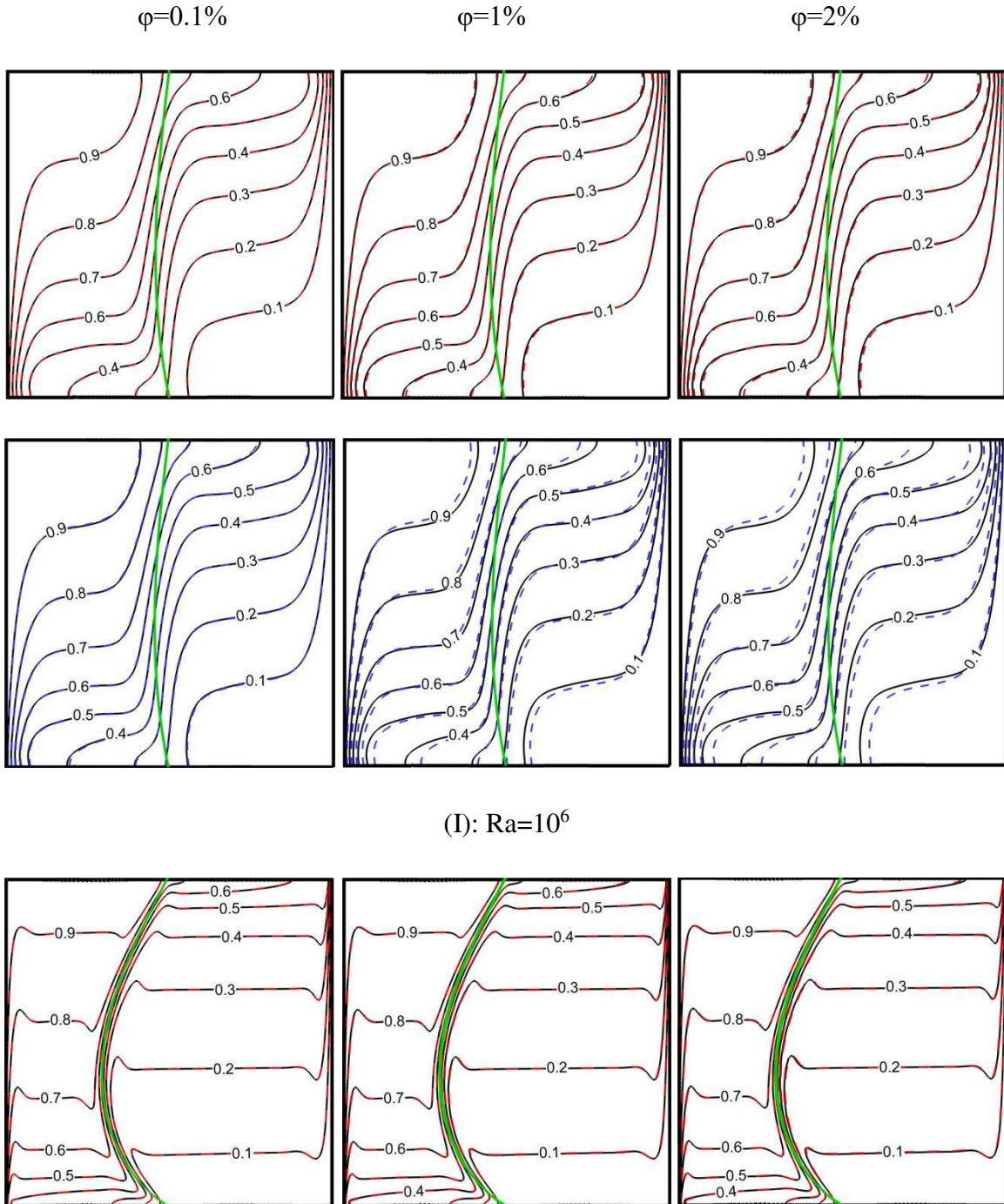


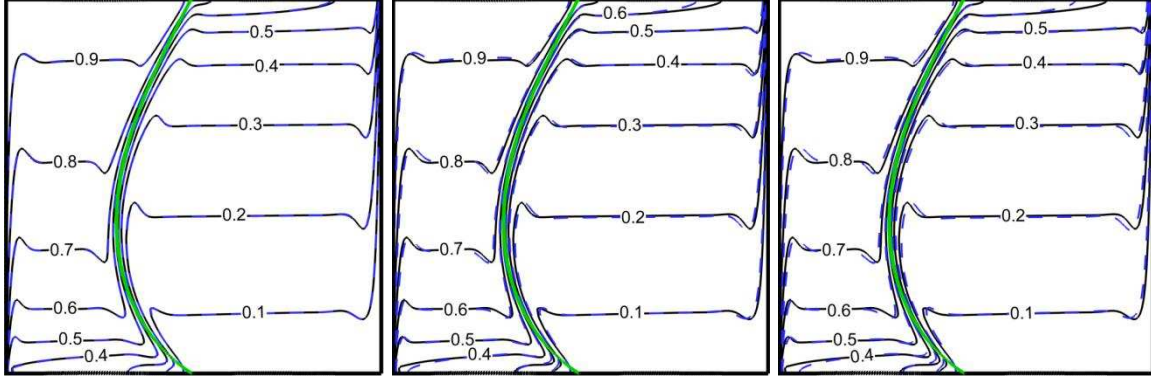
(II): $Ra=10^8$

Fig. 9. The streamlines contours of a: hybrid nanofluid of $Cu-Al_2O_3$ / water and b: nanofluid Al_2O_3 for the various values of ϕ when (I): $Ra=10^6$ and (II) 10^8 for fixed values $\gamma=2\pi/3$ and $Ha=50$

Fig. 10 illustrates the corresponding isotherms contours of the streamlines shown in Fig. 9 for both nanofluid and hybrid nanofluid. As Figs. 10 (I) and (II)-a show, adding Al_2O_3

nanoparticles to the host fluid does not affect the temperature field. Dispersing the nanoparticles of Cu-Al₂O₃ changes the location of the isotherms when Ra=10⁶ and $\phi_{\text{hnf}}=0.01$ and 0.02.





(II): $Ra=10^8$

Fig. 10. The isotherms contours of hybrid nanofluid Cu-Al₂O₃/ water (dashed lines) nanofluid Al₂O₃ (dashed lines) for the various values of ϕ when $Ra=10^6$ and 10^8 for fixed values $\gamma=2\pi/3$ and $Ha=50$

The impacts of Rayleigh and Hartmann numbers on the stream patterns are displayed in Fig. 11 for the picked values of $\gamma=\pi/6$ and $\phi_{nl}=\phi_{hnl}=0.02$. As it is observed, increasing Ra significantly changes the stream patterns. The streamlines are horizontally stretched inside the cold sub-cavity with an increase of Ra . In addition, an increase in fluid flow strength due to the increase of Ra augments the flexible partition displacement. In some cases, the streamlines continue to stretch with increasing Ra until the vortices inside the cold sub-cavity break up into two vortices.

The strength of the vortices created in both the sub-cavities decreases with increasing Ha . The Lorentz force coming from the magnetic field is a drag force acting against the fluid movement. In fact, the magnetic field behaves as an opposite factor to the buoyancy force. Thus, it is justified that the fluid flow strength declines with an increase of Ha . Furthermore, it can be seen that the magnetic field has no effect on the flexible partition deformation at the steady state. In the cases with two or three vortices, an increase of the Hartmann number causes the vortices to approach to each other so that a unique vortex is finally formed. The center of the vortices in the

left and right sub-enclosures swing towards down and up, respectively. The results state that in the similar conditions the fluid flow strength for the single nanofluid is more than that of the hybrid nanofluid. Apparently, the reduction of the hybrid nanofluid flow strength is due to the intense increase of the hybrid nanofluid viscosity as a result of the simultaneous presence of Cu and Al₂O₃ nanoparticles.

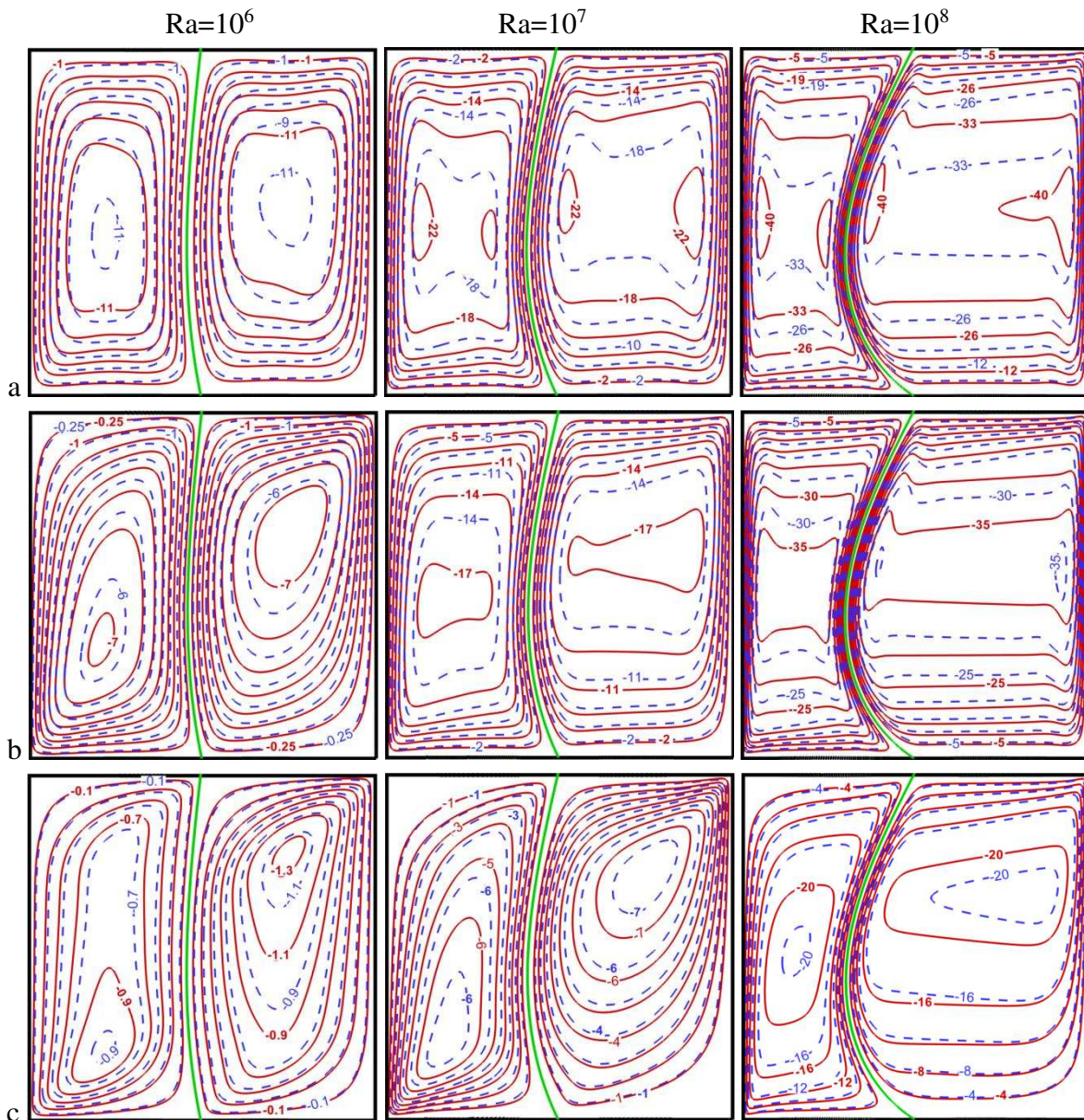
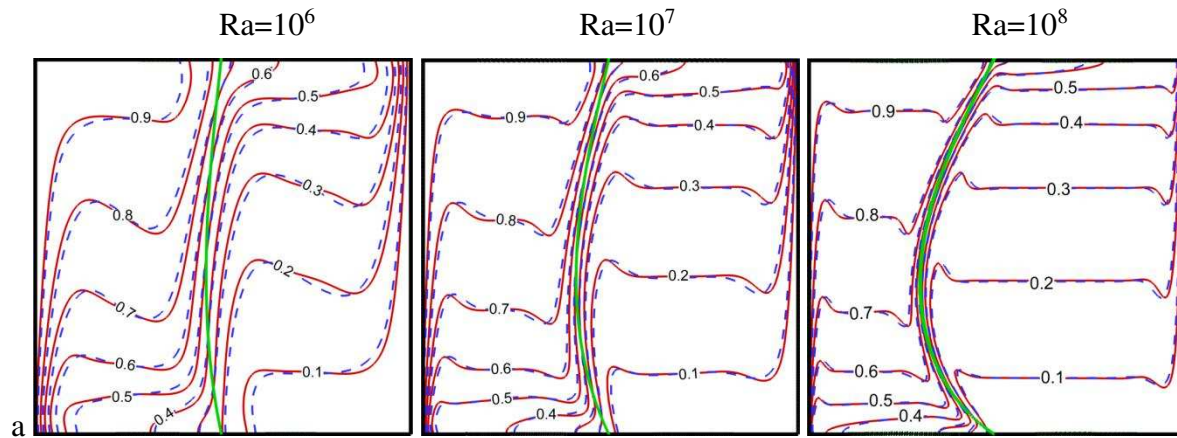


Fig. 11. The streamline contours of hybrid nanofluid (dashed lines) and nanofluid with Al_2O_3 nanoparticles (solid lines) for various values of Ra when: Ha=0, b: Ha=50 c: Ha=200 and $\gamma=\pi/6$ and $\phi_{\text{hnf}}=\phi_{\text{Al}_2\text{O}_3}=2\%$

Fig. 12 shows the isotherms contours relating to the streamlines shown in Fig. 11. These results illustrate that the dominant mechanism of heat transfer varies with the change of Rayleigh number and Hartmann number. The isotherms incline to possess a stratification pattern as Ra augments. In fact, these stratification patterns are formed as a result of the increase of the fluid flow strength. The patterns demonstrate the thermal mixing of fluid. On the other hand, the lines of isotherms contours tend to be parallel to the vertical bounds when Ha increases. In other words, as the magnetic field strength augments, the conduction and advection contributions at heat transfer process increases and decreases, respectively. The isotherms of Ha=200 and $\text{Ra}=10^6$ clearly illustrate that the conduction mode is dominant.



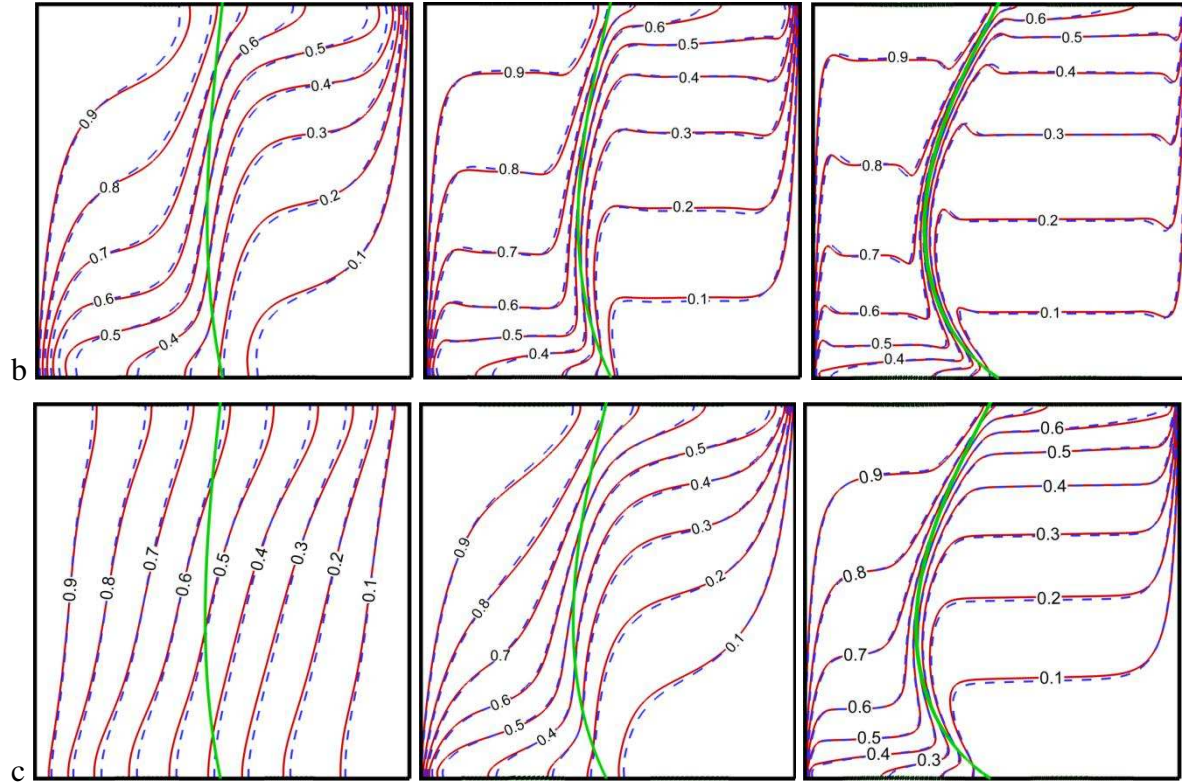
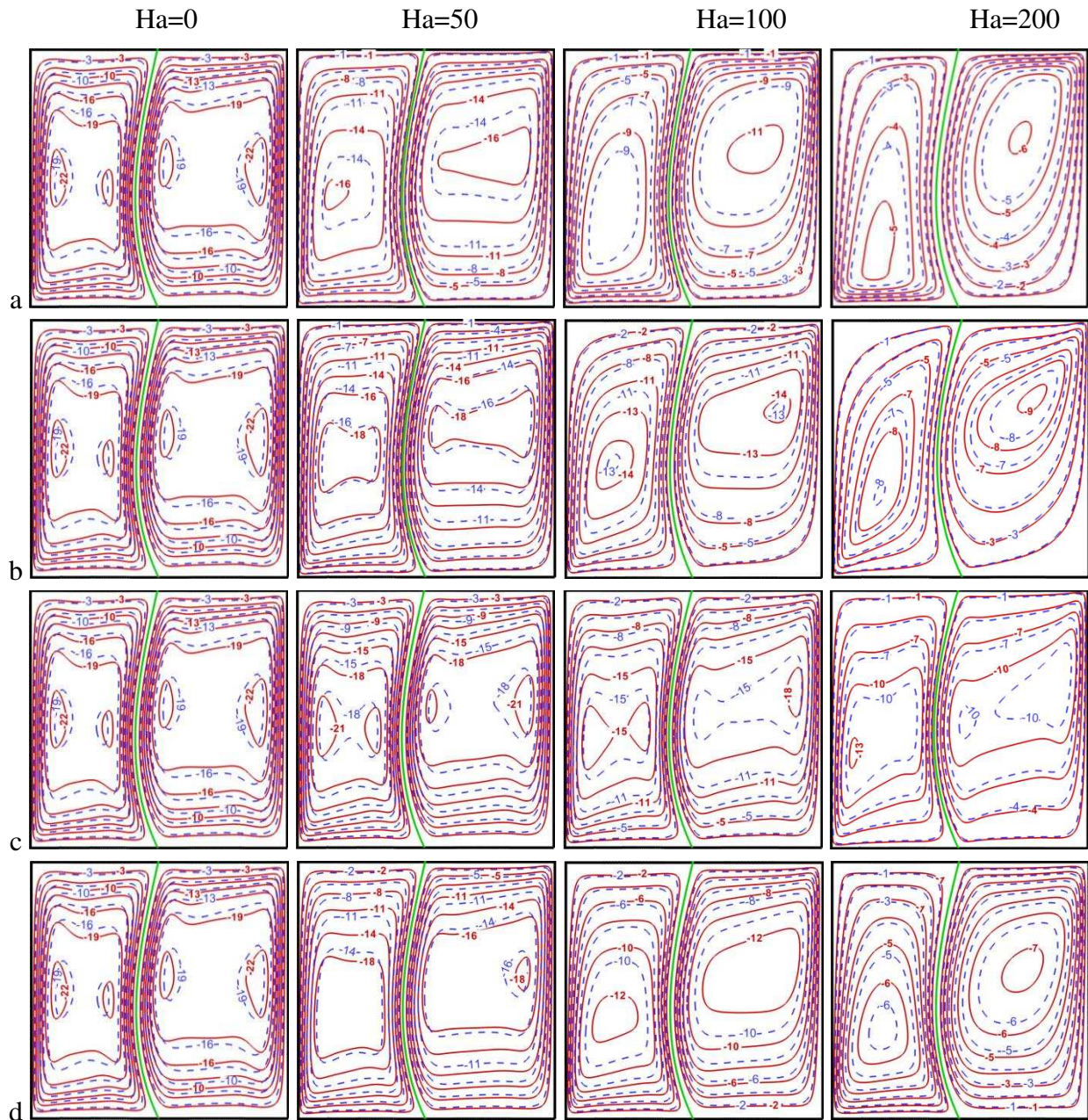


Fig. 12. The isotherms contours of hybrid nanofluid (blue lines) and nanofluid with Al_2O_3 nanoparticles (red lines) for the various values of Ra when: $Ha=0$, b: $Ha=50$ c: $Ha=200$ and $\gamma=\pi/6$ and $\phi_{\text{hnf}} = \phi_{\text{Al}_2\text{O}_3}=2\%$

Fig. 13 depicts the effects of the parameters of magnetic field on the streamlines of the hybrid and single nanofluids. The values of Ra and ϕ are 10^7 and 0.02, respectively. Obviously, the strength of circulation augments as the angle of the magnetic-field inclination, γ , grows by $\pi/2$. After that, the mobility of fluid continuously begins to diminish when γ varies from $\pi/2$ to π . In fact, the vertical component of Lorentz force, which acts as a resistant one against buoyancy term, is reduced as γ increases from $\pi/2$ to π . This component of Lorentz force is exactly zero when $\gamma = \pi/2$. Therefore, it is expected that the buoyancy force has the maximum effects when the magnetic field vector is perpendicular. In addition, the variations of inclination angle γ affect the governing

patterns. The sub-figures shown in Fig. 13 depict that the created secondary vortices in the center of the sub-cavities unify with increasing Ha for all the inclination angles expect $\gamma=\pi/2$. This phenomenon is due to that the drag force of Lorentz has the least impact when it is applied perpendicular. Furthermore, it can be seen that the results are the same for $\gamma=0$ and π . As previously mentioned, the Lorentz force is a periodic one with the period of π .



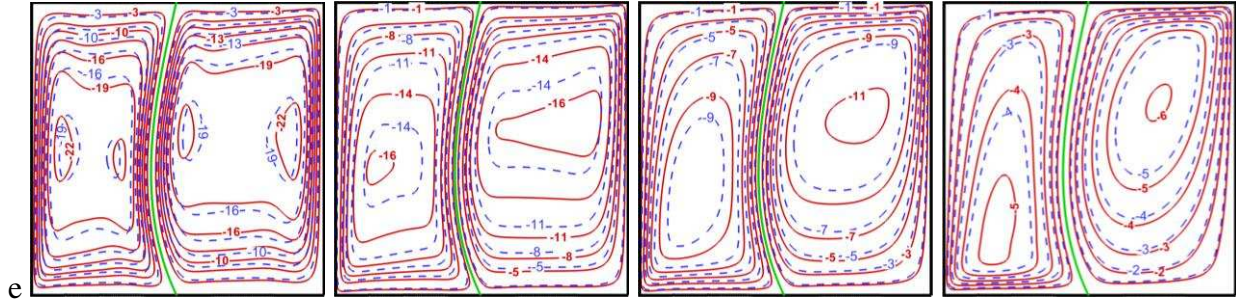
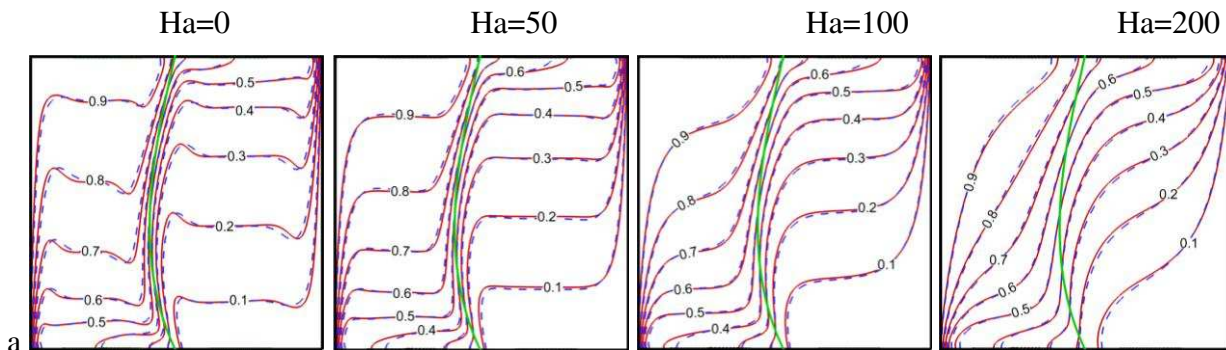


Fig. 13. The streamlines contours of hybrid nanofluid (dashed lines) and nanofluid with Al_2O_3 nanoparticles (solid lines) for different values of Ha in a: $\gamma=0$, b: $\gamma=45$ c: $\gamma=90$ d: $\gamma=135$ e: $\gamma=180$ and $\text{Ra}=10^7$ and $\varphi_{\text{hnf}}=\varphi_{\text{Al}_2\text{O}_3}=2\%$

The effect of γ and Ha on the isotherms are displayed in Fig. 14 for $\text{Ra}=10^7$ and $\varphi_{\text{hnf}}=\varphi_{\text{Al}_2\text{O}_3}=2\%$. When the magnetic field is applied to the flow domain, the fluid thermal mixing is reduced. When $\text{Ra}=10^7$ and $\varphi_{\text{hnf}}=\varphi_{\text{Al}_2\text{O}_3}=2\%$, it is not observed noticeable differences among the isotherms patterns. However, it is worth mentioning that the isotherms of $\gamma=\pi/2$ differ from those of the other values of γ .



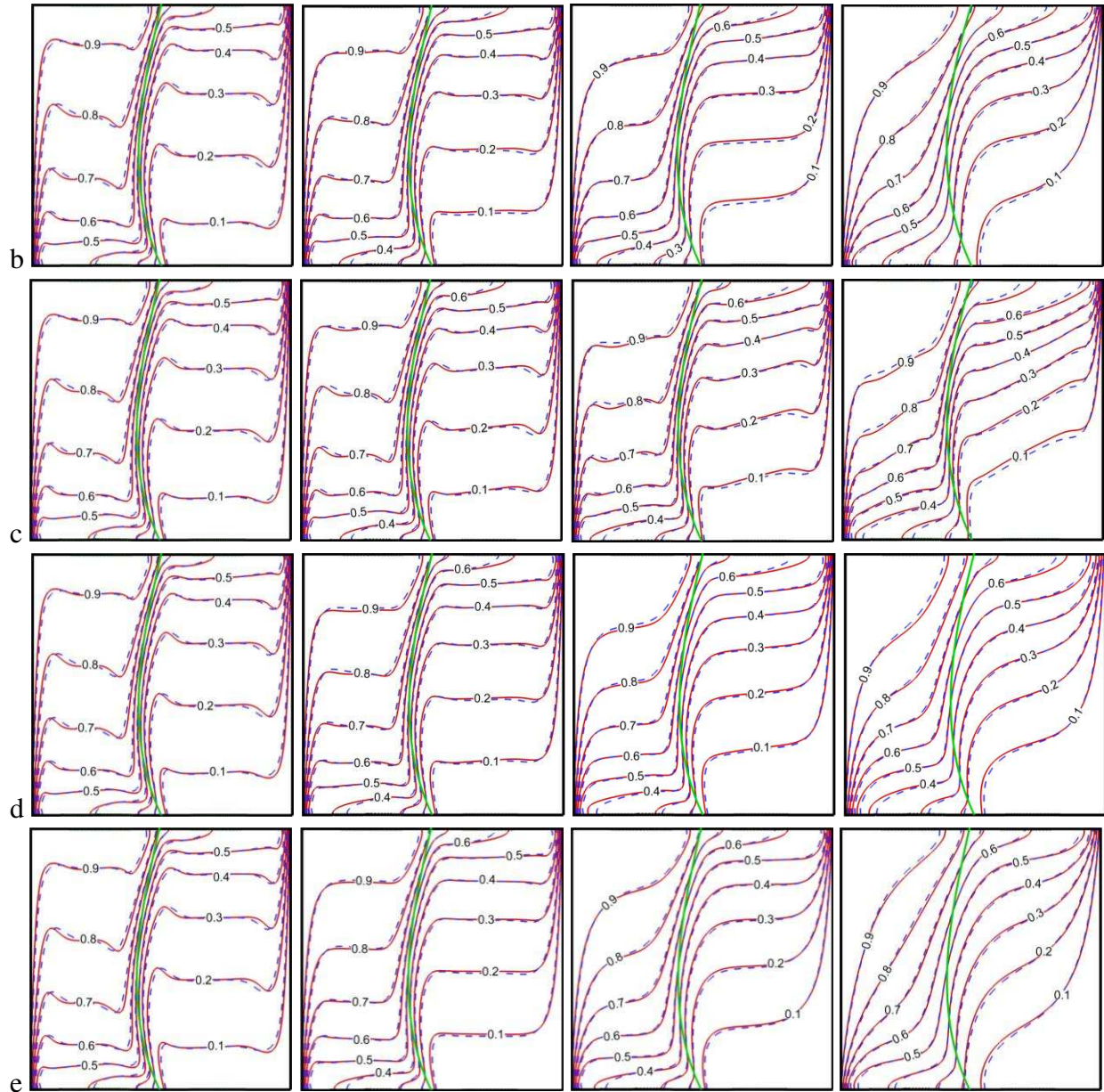


Fig. 14. The isotherms contours of hybrid nanofluid (dashed lines) and nanofluid with Al_2O_3 nanoparticles (solid lines) for different values of Ha in a: $\gamma=0$, b: $\gamma=45$ c: $\gamma=90$ d: $\gamma=135$ e: $\gamma=180$ and $Ra=10^7$ and $\phi_{\text{hnf}}=\phi_{\text{Al}_2\text{O}_3}=2\%$

Figs. 15 (a) and (b) show the variations trend of Nu_{avg} according to γ for different values of Ha . The other parameters are constant so that $Ra=10^8$ and $\phi=2\%$. Nu_{avg} increases as γ increases by $\gamma=\pi/2$. After that, it begins to reduce by $\gamma=\pi$. In other words, the maximum value of Nu_{avg} is at $\gamma=\pi/2$. This result arises from the fact that the fluid flow strength is maximum when $\gamma=\pi/2$. In

addition, Nu_{avg} decreases with the increment of Ha . As said earlier, the mobility of fluid exposed the magnetic field is reduced. Thus, this can justify that an increase in Ha causes a decrease in Nu_{avg} . Finally, the results depict that dispersing Al_2O_3 nanoparticles in the host fluid augments the rate of heat transfer, while $Cu-Al_2O_3$ nanoparticles decline the rate.

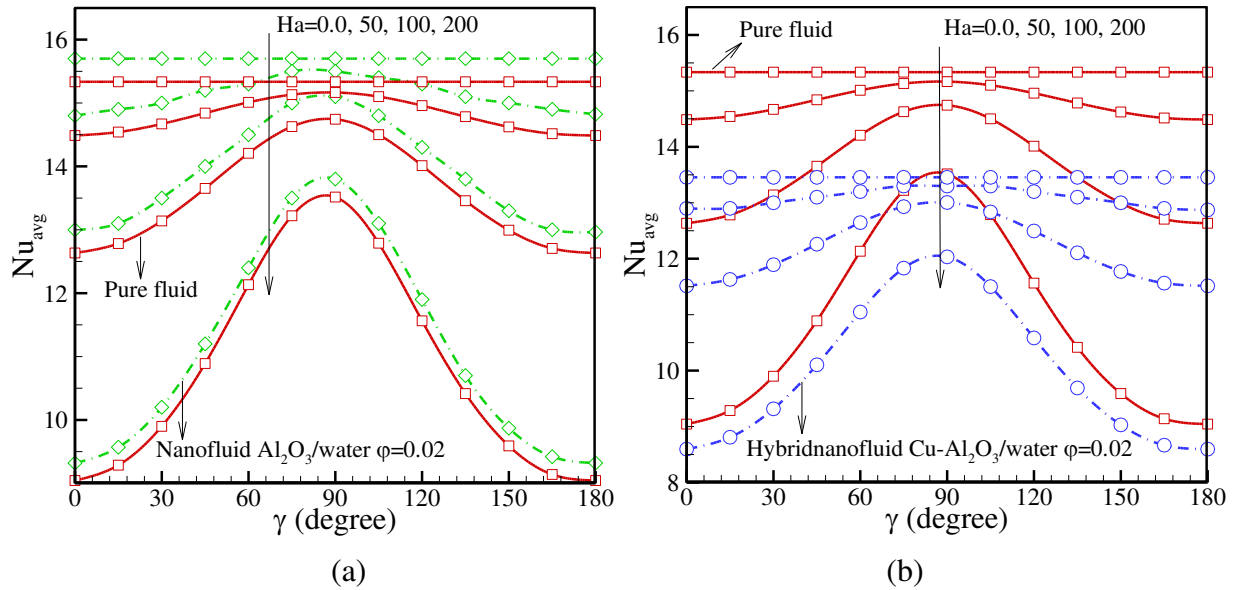


Fig. 15. The effects of Ha and γ on Nu_{avg} for $Ra=10^8$ and $\phi_{hnf} = \phi_{Al_2O_3} = 2\%$

Figs. 16 (a) and (b) illustrate the variations trend of the mean temperature according to γ for different values of Ha . Here, ϕ and Ra are 0.02% and 10^8 , respectively. The results indicate that T_{avg} reduces as γ augments. The T_{avg} variation according to γ is a quasi-sinusoidal function. Further, the amplitude of these quasi-sinusoidal functions increases with the increment of Ha . Fig. 16 (a) clearly indicates that the volume fraction 0.02 for the nanofluid Al_2O_3 / water causes increases in T_{avg} at all γ and Ha values. However, for the hybrid nanofluid $Cu-Al_2O_3$ / water at $Ha=200$, when $0 \leq \gamma < 120$ and $165 < \gamma \leq 180$, the simultaneous presence of Cu and Al_2O_3 raises

T_{avg} . On the other hand, if $120 < \gamma < 165$, the presence of these nanoparticles decreases the mean temperature. Apparently, for all types of fluids when $Ha=100$ or 200 , the maximum and minimum values of T_{avg} occurs at 50° and 140° , respectively.

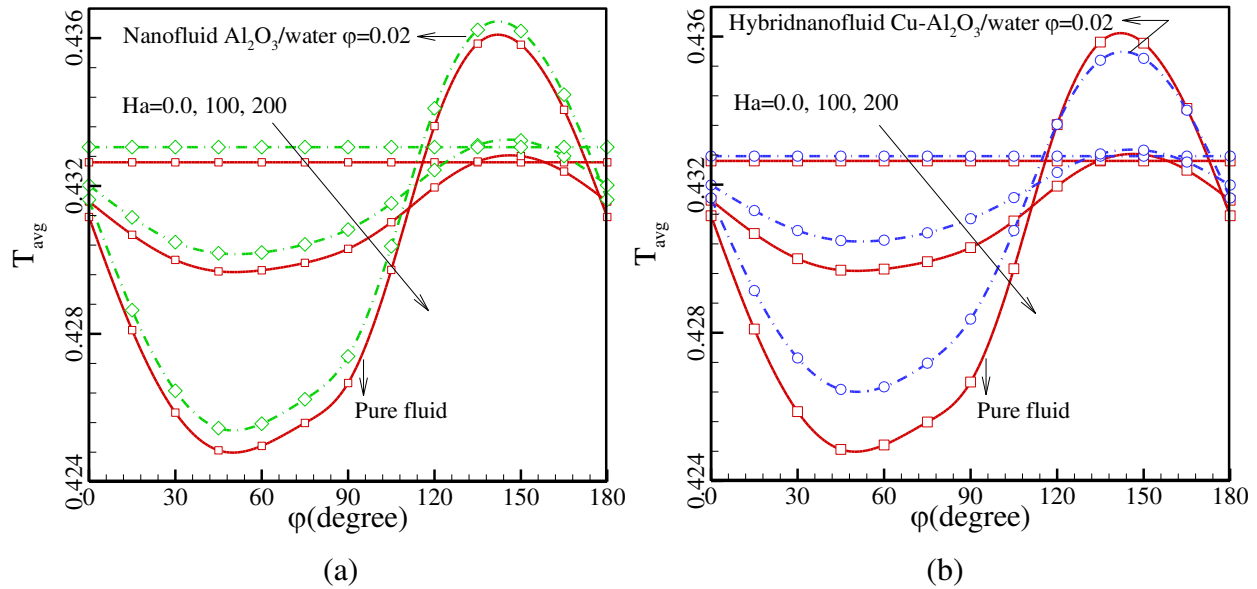


Fig. 16. The effects of Ha and γ on the average temperature T_{avg} for $Ra=10^8$ and $\phi_{hnf} = \phi_{Al_2O_3}=2\%$

Fig. 17 illustrates that σ_{max} increases with an increase of Ha for all types of fluids. It is observed that at the beginning, σ_{max} decreases as γ increases by 30° . After that for $Ha \leq 100$, the maximum stress increases until γ reaches 105° , while for $Ha=200$, the maximum stress occurs around $\gamma=90^\circ$. Then, it can be seen that σ_{max} continuously decreases as γ grows. Figs. 17 (a) and (b) express that the maximum stress imposed on the flexible partition due to the interaction of the pure fluid and the partition is more than that caused via the interaction of the nanofluid/ hybrid nanofluid and the solid.

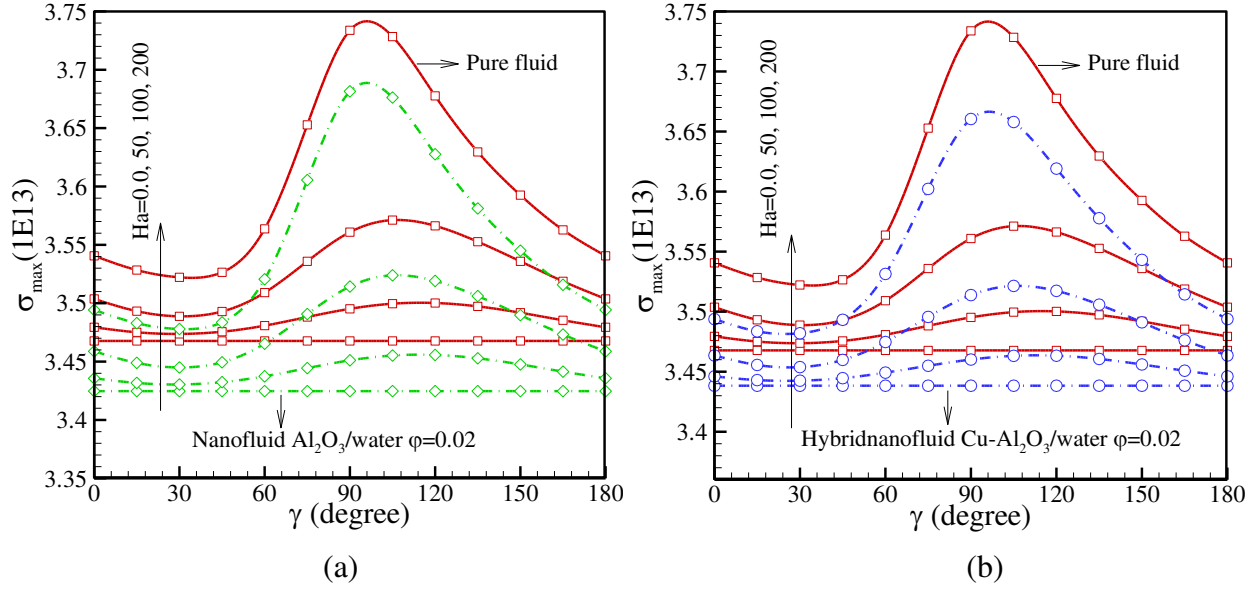


Fig. 17. The effects of Ha and γ on the maximum stress imposed on the partition for $Ra=10^8$ and $\varphi_{hnf} = \varphi_{Al_2O_3} = 2\%$

The effects of Ha and $\varphi_{hnf}/\varphi_{Al_2O_3}$ on Nu_{avg} and T_{avg} at the fixed values of $Ra=10^7$ and $\gamma=2\pi/3$ are presented in Fig. 18 (a) and (b). The examined values for the volume fractions are 1 and 2 %. It is obvious that an increase in Ha increases and decreases the average temperature and Nusselt number, respectively. As previously mentioned, the magnetic field acts as a drag force against the fluid flow. Accordingly, increasing the value of Ha means augmentation in the drag force acting against the advection mechanism. In general, it can be said that for a specific volume fraction, the reduction of Nu_{avg} or augmentation of T_{avg} with increasing values of Ha for the nanofluid Al_2O_3 is more than that for the hybrid nanofluid $Cu-Al_2O_3$. From Fig. 18 (a), increasing the volume fraction of the single and hybrid nanofluids increases and decreases Nu_{avg} , respectively. In order to justify this outcome, it can be said that the increase of the hybrid nanofluid viscosity due to the simultaneous presence of Cu and Al_2O_3 nanoparticles is extremely larger than the increase of the other thermophysical properties especially the thermal conduction. Therefore, as previously seen,

the intense reduction of the mobility of the hybrid nanofluid due to the intense increase of viscosity can be the reason for decreasing Nu_{avg} . Also, from Fig. 18 (b) it is concluded that the presence of Al_2O_3 and $Cu-Al_2O_3$ nanoparticles at $Ra=10^7$ and $\gamma=2\pi/3$ increases and decreases the average temperature of the fluid, respectively.

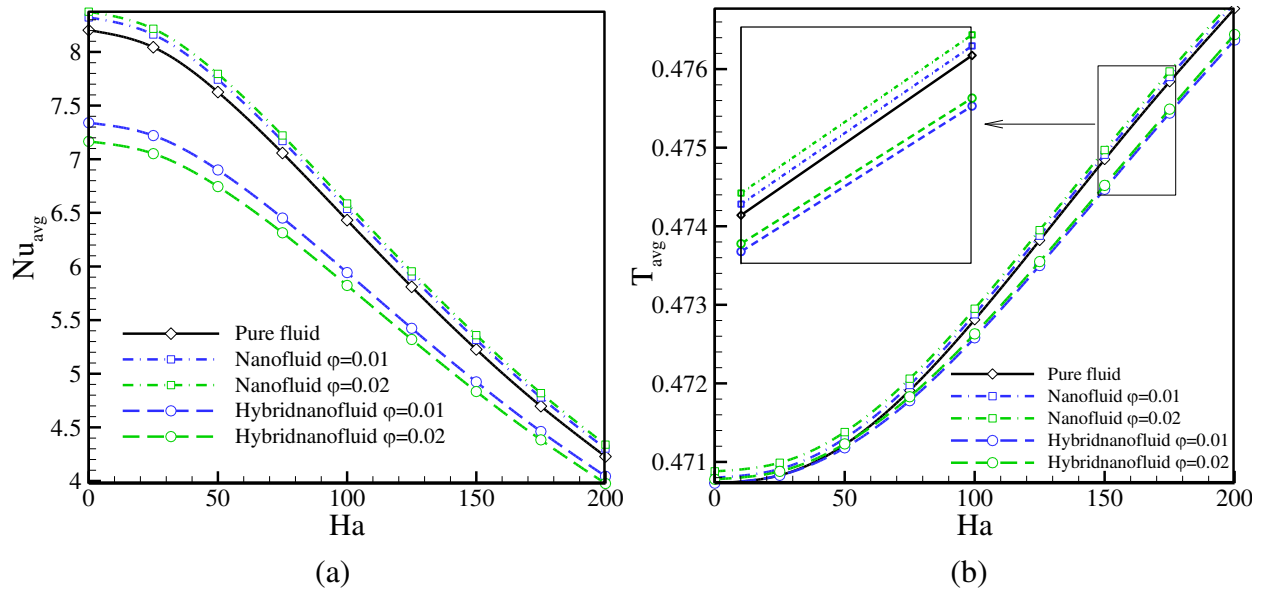


Fig. 18. The effects of Ha and ϕ on a: the Nusselt number b: the average temperature in $Ra=10^7$, $\gamma=2\pi/3$

Fig. 19 illustrates that for all types of fluids an increase in Ha increases σ_{max} when $Ra=10^7$ and $\gamma=2\pi/3$. On the other hand, the use of Al_2O_3 and $Cu-Al_2O_3$ nanoparticles decreases σ_{max} . Nevertheless, it cannot be said with certainty that which type of nanofluids reduce σ_{max} more. Generally, when $Ha \geq 100$ and for different values of ϕ , σ_{max} for the single and hybrid nanofluids are the same.

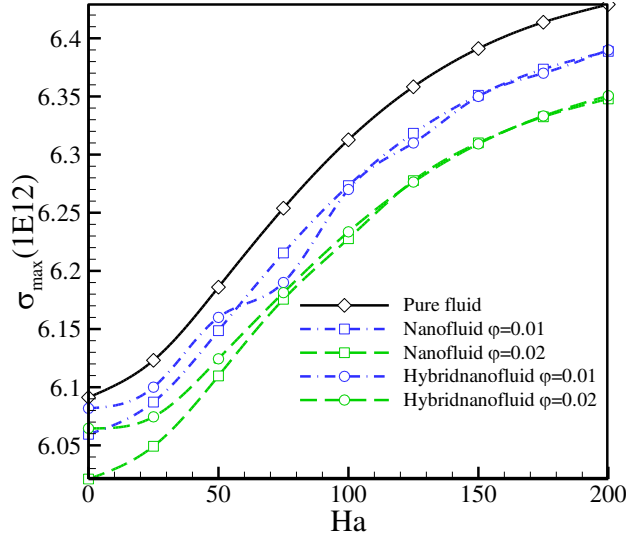


Fig. 19. The effects of Ha and ϕ on the maximum stress imposed on the partition at $Ra=10^7$ and $\gamma=2\pi/3$

Comparison of Nu_{avg} of the single and hybrid nanofluids for different values of Ra and ϕ is presented in Table 2. The other parameters are selected constant so that $Ha=50$ and $\gamma=\pi/3$. The data presented in Table 3 indicates that for all Ra values and both types of nanofluids, the Nu_{av} is decreased when $\phi=0.1$. Moreover, increasing the volume fraction of nanoparticles Al_2O_3 and Al_2O_3-Cu enhances and declines the Nu_{avg} , respectively. The data also indicate that an increase in Ra extremely augments the heat transfer rate.

Table 4. Comparison of Nu_{avg} of the single and hybrid nanofluids for various values of Ra and ϕ when $Ha=50$ and $\gamma=\pi/3$

ϕ (%)	$Ra=10^6$		$Ra=10^7$		$Ra=10^8$	
	$Al_2O_3/water$	$Cu-Al_2O_3/water$	$Al_2O_3/water$	$Cu-Al_2O_3/water$	$Al_2O_3/water$	$Cu-Al_2O_3/water$
0.0	3.5920	3.5920	7.6867	7.6867	15.011	15.011
0.1	3.5827	3.5489	7.6631	7.5786	14.963	14.79
0.33	3.5991	3.4924	7.7002	7.4394	15.036	14.508
0.75	3.6367	3.374	7.7855	7.151	15.207	13.928
1	3.6479	3.2904	7.8045	6.9502	15.241	13.525

2	3.6741	3.2201	7.8579	6.7946	15.344	13.228
---	--------	--------	--------	--------	--------	--------

The data presented in Table 5 give information on the mean temperature variations with Ra and ϕ when Ha=50 and $\gamma=\pi/3$. Clearly, dispersing the single and hybrid nanoparticles in the host fluid increase T_{avg} . Moreover, the results demonstrate that the increase of T_{avg} due to adding the hybrid nanoparticles is more than that for the single nanoparticles. Also, an increase in Ra extremely reduces T_{avg} .

Table 5. Comparison of the average temperature between the nanofluid Al₂O₃-water and Al₂O₃-Cu/water for different values of Ra and ϕ

ϕ (%)	Ra=10 ⁶		Ra=10 ⁷		Ra=10 ⁸	
	Al ₂ O ₃ /water	Cu-Al ₂ O ₃ /water	Al ₂ O ₃ /water	Cu-Al ₂ O ₃ /water	Al ₂ O ₃ /water	Cu-Al ₂ O ₃ /water
0.0	0.48600	0.48600	0.46966	0.46966	0.43180	0.43180
0.1	0.48601	0.48605	0.46968	0.4697	0.43182	0.43181
0.33	0.48603	0.48613	0.4697	0.46976	0.43187	0.43185
0.75	0.48606	0.48628	0.46973	0.46987	0.43195	0.43192
1	0.4861	0.48637	0.46977	0.46993	0.432	0.43196
2	0.48617	0.48653	0.46987	0.47004	0.43223	0.43213

The results given in Table 6 explain that at Ha=50 and $\gamma=\pi/3$, the maximum stress occurring in the flexible partition increases when Ra increases. In contrast, increasing the volume fraction of single and hybrid nanoparticles decreases the induced maximum stress. In fact, an increase in Ra makes an increase in the mobility of fluid, consequently, increases the interaction between the fluid and solid. Also, comparison of the results shows that the maximum stress at the flexible partition of cavity filled with the hybrid nanofluid is more than that of cavity occupied using the single nanofluid.

Table 6. Comparison of the maximum value of stress in flexible partition between the nanofluid Al_2O_3 -water and Al_2O_3 -Cu/water for various values of Ra and ϕ when $\text{Ha}=50$ and $\gamma=\pi/3$

ϕ (%)	$\text{Ra}=10^6$		$\text{Ra}=10^7$		$\text{Ra}=10^8$	
	$\text{Al}_2\text{O}_3/\text{water}$	$\text{Cu-Al}_2\text{O}_3/\text{water}$	$\text{Al}_2\text{O}_3/\text{water}$	$\text{Cu-Al}_2\text{O}_3/\text{water}$	$\text{Al}_2\text{O}_3/\text{water}$	$\text{Cu-Al}_2\text{O}_3/\text{water}$
0.0	1.1845E12	1.1845E12	6.1810E12	6.1810E12	3.4809E13	3.4809E13
0.1	1.1838E12	1.1839E12	6.1774E12	6.1703E12	3.4789E13	3.4800E13
0.33	1.1823E12	1.1826E12	6.1604E12	6.1648E12	3.4738E13	3.4768E13
0.75	1.1796E12	1.1802E12	6.1448E12	6.1544E12	3.4645E13	3.4712E13
1	1.1781E12	1.1788E12	6.146E12	6.1482E12	3.4597E13	3.4678E13
2	1.1713E12	1.1735E12	6.098E12	6.1352E12	3.4374E13	3.4493E13

Conclusion

Unsteady natural convection within an enclosure equally divided by a flexible partition is numerically investigated utilizing the Galerkin finite element method. The enclosure occupied by the hybrid nanofluid is under the influence of a uniform magnetic field. The effects of different parameters including the Hartmann number Ha , the Rayleigh number Ra , the nanoparticles concentration ϕ and the angle of the magnetic field vector γ on the flow strength, the rate of heat transfer and the stress of flexible partition are studied. The main findings of the current work are summarized as follows:

- 1-The strength of the hybrid and regular nanofluids circulation augments as the magnetic field vector angle γ augments until γ reaches $\pi/2$. Then, the mobility of fluid begins to vanish when γ varies from $\pi/2$ to π . The impact of magnetic field on the mean Nusselt number Nu_{avg} is the maximum at $\gamma = \pi/2$.
- 2- Comparing to the base fluid,, Nu_{avg} increases for the nanofluids with volume fraction 0.02 of Al_2O_3 , but decreases for Cu- Al_2O_3 nanoparticles. Moreover, the presence of Al_2O_3

nanoparticles enhances the fluid flow strength while the combination of Cu and Al₂O₃ nanoparticles (hybrid nanoparticles) results in the reduction of circulation strength. The reduction of Nu_{avg} is mainly due to the significant increase of the dynamic viscosity of hybrid nanofluids.

3- The maximum stress imposed on the flexible partition coming from the pure fluid and the partition interaction is larger than that of the solid and regular/ hybrid nanofluid interaction. Therefore, it is concluded that the presence of nanoparticles would cause smaller partition deflection compared to the case of pure fluid.

4- The vortices strength inside both the sub-cavities decreases with the increase of Ha. However, the fluid flow strength rises as Ra increases. Moreover, the dominant mechanism of heat transfer changes with Ra and Ha values. The presence of hybrid nanoparticles in the host fluid (water) results in a fluid with higher dynamic viscosity and thermal conductivity. The increase of the thermal conductivity tends to enhance the natural convective heat transfer; in contrast, the augmentation of the dynamic viscosity tends to decrease the heat transfer. The results reveal that the overall effect of dispersing hybrid nanoparticles in the host fluid is the reduction of Nu_{avg}. However, the presence of the same amount of single Al₂O₃ nanoparticles would enhance Nu_{avg}.

Acknowledgement

This project is supported by 111 project (B18002)

References

- [1] Yang, K.T., 1987. Natural convection in enclosures. Handbook of Single-Phase Heat Transfer, pp.13-1.
- [2] M. Sheikholeslami, Soleimani, S. and Ganji, D.D., Effect of electric field on hydrothermal behavior of nanofluid in a complex geometry. Journal of Molecular Liquids, 213 (2016) 153-161.
- [3] A. Al-Mudhaf, A.J. Chamkha, Natural Convection of Liquid Metals in an Inclined Enclosure in the Presence of a Magnetic Field, Int. J. Fluid Mech. Res., 31 (2004) 221-243.
- [4] O.D. Makinde, F. Mabood, W. A. Khan, and M. S. Tshehla. MHD flow of a variable viscosity nanofluid over a radially stretching convective surface with radiative heat. Journal of Molecular Liquids 219 (2016) 624-630.
- [5] R.S. Kaluri, R. Anandalakshmi, T. Basak, Bejan's heatline analysis of natural convection in right-angled triangular enclosures: Effects of aspect-ratio and thermal boundary conditions, Int. J. Therm. Sci. 49 (2010) 1576–1592
- [6] A. Al-Mudhaf, A.J. Chamkha, Natural Convection of Liquid Metals in an Inclined Enclosure in the Presence of a Magnetic Field, Int. J. Fluid Mech. Res., 31 (2004) 221-243.
- [7] M. Sathiyamoorthy and A.J. Chamkha, Effect of Magnetic Field on Natural Convection Flow in a Square Cavity for Linearly Heated Side Wall(s), Int. J. Therm. Sci., 49 (2010) 1856-1865.
- [8] M. Sathiyamoorthy and A.J. Chamkha, Natural Convection Flow under Magnetic Field in a Square Cavity for Uniformly (or) Linearly Heated Adjacent Walls, Int. J. Numer. Methods Heat & Fluid Flow, 22 (2012) 677-698.
- [9] M. Sheikholeslami, M. M. Rashidi, T. Hayat, and D. D. Ganji. Free convection of magnetic nanofluid considering MFD viscosity effect, Journal of Molecular Liquids, 218 (2016) 393-399.
- [10] M. Sheikholeslami and D. D. Ganji. Nanofluid hydrothermal behavior in existence of Lorentz forces considering Joule heating effect, Journal of Molecular Liquids 224 (2016) 526-537.

- [11] M. Sheikholeslami, Influence of magnetic field on nanofluid free convection in an open porous cavity by means of Lattice Boltzmann method, *Journal of Molecular Liquids* 234 (2017) 364-374.
- [12] A. Ben-Nakhi, A.J. Chamkha, Conjugate natural convection in a square enclosure with inclined thin fin of arbitrary length, *Int. J. Thermal Sci.* 46, (2007) 467–478.
- [13] Sheikholeslami, M., and D. D. Ganji, Free convection of Fe₃O₄-water nanofluid under the influence of an external magnetic source, *Journal of Molecular Liquids* 229 (2017): 530-540.
- [14] N. Ben Cheikh, A.J. Chamkha, and B. Ben Beya, Effect of inclination on heat transfer and fluid flow in a finned enclosure filled with a dielectric liquid, *Numer. Heat Transfer Part A* 56 (2009) 286–300.
- [15] A.J. Chamkha, M. Mansour, S.E. Ahmed, Double diffusive natural convection in inclined finned triangular porous enclosures in the presence of heat generation/absorption effects, *Heat Mass Transfer* 46 (2010) 757–768.
- [16] K.S. Chen, A.C. Ku, C.H. Chou, Investigation of natural convection in partially divided rectangular enclosures both with and without an opening in the partition plate: Measurement results, *J. Heat Transfer* 112 (1990) 648–652.
- [17] E. Bilgen, Natural convection in enclosures with partial partitions, *Ren. En.* 26 (2002) 257–270.
- [18] H.F. Oztop, I. Dagtekin, Natural convection heat transfer by heated partitions within enclosures, *Int. Comm. Heat Mass Transfer* 28 (2001) 823–834.
- [19] M.W. Nanstell, R. Greif, Natural convection in undivided and partially divided rectangular enclosures, *J. Heat Transfer* 103 (1981) 623–629.
- [20] M.W. Nanstell, R. Greif, An investigation of natural convection in enclosures with two and three dimensional partitions, *Int. J. Heat Mass Transfer* 27 (1984) 561–571.

- [21] Y. Varol, H.F. Oztop, A. Varol, Effects of thin fin on natural convection in porous triangular enclosures, *Int. J. Therm. Sci.* 46 (2007) 1033–1045.
- [22] S. A. M. Mehryan, F. M. Kashkooli, M. Ghalambaz, A. J. Chamkha, Free convection of hybrid Al₂O₃-Cu water nanofluid in a differentially heated porous cavity. *Advanced Powder Technology* 28(9) (2017) 2295-2305.
- [23] H. Zargartalebi, M. Ghalambaz, A. Chamkha, I. Pop, A.S. Nezhad, Fluid-structure interaction analysis of buoyancy-driven fluid and heat transfer through an enclosure with a flexible thin partition. *International Journal of Numerical Methods for Heat & Fluid Flow*, 28(9) (2018) 2072-2088.
- [24] E. Jamesahar, E., M. Ghalambaz, A.J. Chamkha, Fluid–solid interaction in natural convection heat transfer in a square cavity with a perfectly thermal-conductive flexible diagonal partition. *International Journal of Heat and Mass Transfer* 100 (2016) 303-319.
- [25] S. A. M. Mehryan, M. Ghalambaz, M. A. Ismael, A. J. Chamkha, Analysis of fluid-solid interaction in MHD natural convection in a square cavity equally partitioned by a vertical flexible membrane. *Journal of Magnetism and Magnetic Materials* 424 (2017) 161-173.
- [26] Feng Xu, John C. Patterson, Chengwang Lei, Heat transfer through coupled thermal boundary layers induced by a suddenly generated temperature difference, *International Journal of Heat and Mass Transfer* 52 (2009) 4966–4975.
- [27] N. Tatsuo , M. Shiraishi, F. Nagasawa, Y. Kawamura, Natural convection heat transfer in enclosures with multiple vertical partitions, *International journal of heat and mass transfer* 31 (8) (1988) 1679-1686.
- [28] H.F. Oztop, Y.Varol, A. Koca, Natural convection in a vertically divided square enclosure by a solid partition into air and water regions, *Int. J. Heat Mass Transfer*, 52 (2009) 5909–5921.
- [29] K. Kahveci, Natural Convection in a Partitioned Vertical Enclosure Heated With a Uniform Heat Flux, *ASME Journal of Heat Transfer*, 129 (2007) 717-726.

- [30] K. Kahveci, Buoyancy Driven Heat Transfer of Nanofluids in a Tilted Enclosure, *Journal of Heat Transfer*, JUNE 2010, Vol. 132 / 062501-1.
- [31] P.K. Jeena, E.A. Brocchi, M.S. Motta, In-situ formation of Cu–Al₂O₃ nanoscale composites by chemical routes and studies on their microstructures, *Material Science and Engineering A313* (2001) 180–186.
- [32] S. Suresha, K.P. Venkitaraja, P. Selvakumara, M. Chandrasekar, Synthesis of Al₂O₃–Cu/water hybrid nanofluids using two step method and its thermo physical properties, *Colloids and Surfaces A: Physicochem. Eng. Aspects* 388 (2011) 41–48.
- [33] S. Suresh, K.P. Venkitaraj, P. Selvakumar, M. Chandrasekar, Effect of Al₂O₃–Cu/water hybrid nanofluid in heat transfer, *Exp. Thermal Fluid Sci.* 38 (2012) 54–60.
- [34] M.H. Esfe, A.A.A. Arani, M Rezaie, W.M. Yan, A. Karimipour, Experimental determination of thermal conductivity and dynamic viscosity of Ag–MgO/water hybrid nanofluid, *International Communications in Heat and Mass Transfer* 66 (2015) 189–195.
- [35] A. Moghadassi, E. Ghomi, F. Parvizian, A numerical study of water based Al₂O₃ and Al₂O₃–Cu hybrid nanofluid effect on forced convective heat transfer, *International Journal of Thermal Sciences* 92 (2015) 50–57.
- [36] GH.R. Kefayati, Effect of a magnetic field on natural convection in an open cavity subjugated to water/alumina nanofluid using Lattice Boltzmann method, *International Communications in Heat and Mass Transfer* 40(2013), 67–77.
- [37] H.M. Elshehabey, F.M. Hady, S.E. Ahmed, R.A. Mohamed Numerical investigation for natural convection of a nanofluid in an inclined L-shaped cavity in the presence of an inclined magnetic field, *International Communications in Heat and Mass Transfer* 57 (2014) 228–238.
- [38] R. Nasrin, M.A. Alim, Free convective flow of nanofluid having two nanoparticles inside a complicated cavity, *International Journal of Heat and Mass Transfer* 63 (2013) 191–198.
- [39] J. C. Maxwell, *A Treatise on Electricity and Magnetism*, Oxford University Press, Cambridge, UK, 2nd edition, 1881.

- [40] S.M.S. Murshed, K.C. Leong, C. Yang, Enhanced thermal conductivity of TiO₂—water based nanofluids, *International Journal of Thermal Sciences* 44 (2005) 367–373.
- [41] A. Einstein, *Investigation on the Theory of Brownian Motion*, Dover, New York, NY, USA, 1956.
- [42] H. C. Brinkman, The viscosity of concentrated suspensions and solutions, *The Journal of Chemical Physics*, vol. 20, no. 4, pp. 571–581, 1952.
- [43] G. K. Batchelor, The effect of Brownian motion on the bulk stress in a suspension of spherical particles, *Journal of Fluid Mechanics*, vol. 83, no. 1, pp. 97–117, 1977.
- [44] O. Zienkiewicz, R. Taylor, P. Nithiarasu, *The Finite Element Method for Fluid Dynamics 7th Edition*, 2013, Elsevier Science, Butterworth-Heinemann.
- [45] U. Küttler, W. A. Wall, Fixed-point fluid–structure interaction solvers with dynamic relaxation, *Comput Mech* 43 (2008) 61–72.
- [46] Churchill, S. W., Free convection in layers and enclosures. *Heat exchanger design handbook*, 2 (8) (1983).